# Structural transition of solvated H-Ras/GTP revealed by molecular dynamics simulation and local network entropy

Matsunaga, Shota ; Hano, Yuta ; Saito, Yuta ; Fujimoto, Kazuhiro J. ; Kumasaka, Takashi ; Matsumoto, Shigeyuki ; Kataoka, Tohru ; Shima, Fum…

(Citation)
Journal of Molecular Graphics and Modelling,77:51-63

(Issue Date)
2017-10

(Resource Type)
journal article

(Version)
Accepted Manuscript



(URL)
https://hdl.handle.net/20.500.14094/90004653

# Structural transition of solvated H-Ras/GTP revealed by molecular dynamics simulation and local network entropy

Shota Matsunaga, Yuta Hano, Yuta Saito

*Department of Computational Science, Graduate School of System Informatics, Kobe University, 1-1 Rokkodai-cho, Nada-ku, Kobe 657-8501, Japan*

Kazuhiro J. Fujimoto

*Faculty of Pharmaceutical Sciences, Hokuriku University, Ho-3 Kanagawa-machi, Kanazawa 920-1181, Japan*

Takashi Kumasaka

*Protein Crystal Analysis Division, Japan Synchrotron Radiation Research Institute (JASRI), SPring-8, 1-1-1 Kouto, Sayo-cho, Sayo-gun, Hyogo 679-5198, Japan*

Shigeyuki Matsumoto, Tohru Kataoka

*Division of Molecular Biology, Department of Biochemistry and Molecular Biology, Graduate School of Medicine, Kobe University, 7-5-1 Kusunoki-cho, Chuo-ku, Kobe 650-0017, Japan*

Fumi Shima

*Division of Molecular Biology, Department of Biochemistry and Molecular Biology, Graduate School of Medicine, Kobe University, 7-5-1 Kusunoki-cho, Chuo-ku, Kobe 650-0017, Japan; Drug Discovery Science, Division of Advanced Medical Science, Department of Science, Technology and Innovation, Graduate School of Science, Technology and Innovation, Kobe University, 7-5-1 Kusunoki-cho, Chuo-ku, Kobe 650-0017, Japan*

Shigenori Tanaka

*Department of Computational Science, Graduate School of System Informatics, Kobe University, 1-1 Rokkodai-cho, Nada-ku, Kobe 657-8501, Japan*

*Email address:* tanaka2@kobe-u.ac.jp; Fax:+81-78-803-6621 (Shigenori Tanaka)

**Abstract**

The state transitions of solvated H-Ras protein with GTP were theoretically analyzed through molecular dynamics (MD) simulations. To accelerate the structural changes associated with the locations of two switch regions (I and II), the Parallel Cascade Selection MD (PaCS-MD) method was employed in this study. The interconversions between the State 1 and State 2 were thus studied in atomic details, leading to a reasonable agreement with experimental observations and consequent scenarios concerning the transition mechanism that would be essential for the development of Ras inhibitors as anti-cancer agents. Furthermore, the state-transition-based local network entropy (SNE) was calculated for the transition process from State 1 to State 2, by which the temporal evolution of information entropy associated with the dynamical behavior of hydrogen bond network composed of hydration water molecules was described. The calculated results of SNE thus proved to provide a good indicator to detect the dynamical state transition of solvated Ras protein system (and probably more general systems) from a viewpoint of nonequilibrium statistical thermodynamics.

*Keywords:* Ras; Molecular switch; Structural transition; Molecular dynamics; State-transition-based local network entropy

## 1. Introduction

Small GTPases Ras (H-, K-, and N-Ras), the products of the *ras* proto-oncogenes function as guanine nucleotide-dependent molecular switches regulating cell growth, development and apoptosis by cycling between GTP-bound (Ras/GTP) and GDP-bound (Ras/GDP) forms [1–10]. The active Ras transmits the biological signals in the intracellular network to the downstream effectors. The Ras proteins are frequently activated too much in a wide variety of human cancers, making them some of the most promising targets for anti-cancer drug development. The Ras/GTP adopts two inter-converting conformational states, State 1 and State 2, corresponding to inactive and active forms, respectively [1, 6]. Since the State 1 (open) conformation possesses the drug-accessible surface pockets between the two switch regions, named Switch I (residues 32-38) and Switch II (residues 60-75), the information on the transition mechanism between the two states is essential for the efficient development of Ras-specific inhibitors. Much efforts have thus been focused on the elucidation of the structural transitions of Ras proteins employing the experimental techniques such as X-ray crystallography and NMR [6, 8, 10].

In the present study we investigate the state transition mechanism of H-Ras/GTP mainly using the molecular dynamics (MD) simulation method [11–15]. First, we perform Parallel Cascade Selection MD (PaCS-MD) simulations [16] in order to yield the conformational transitions in relatively short computational time. The PaCS-MD was designed to accelerate the dynamical process to reach target structures so that we could easily find the conformational transition between two states. Analyzing the MD trajectories

in comparison with experimental observations [10], we can thus investigate the molecular mechanism of state transition in a direct and detailed manner. Second, we study the relationship between the hydrogen bond network composed of tightly bound water molecules around Ras protein and the state transition in light of information entropy. The state-transition-based local network entropy (SNE) [17–32] is employed as a dynamical measure to detect the state transition in an indirect manner. Through this analysis, we can identify the hydration waters and hydrogen bonds closely linked to the state transition. These theoretical knowledges are expected to provide deeper insights into the state transition mechanism of Ras in conjunction with experimental observations.

In the following Sec. 2, the computational methods used in this study are explained in detail. The calculated results and associated discussions are given in Sec. 3, first on the state transitions observed in Ras proteins and secondly on the temporal variations of SNE related to the dynamics of hydrogen bond network. Section 4 concludes with summary.

## 2. Computational methods

### *2.1. Structure preparation*

The structural transition between State 1 and State 2 of Ras protein is characterized in terms of the open and closed forms of Switch I and Switch II. In this paper the Switch I and II regions are identified as the residues 32-38 and 60-75, respectively. In order to specify the structural features of Ras protein, we introduce two distance parameters (reaction coordinates), $dT$ and $dY$ (see Fig. 1): The former is defined by the distance between

the oxygen (OG1) atom of Thr35 and the phosphorus (PG) atom of GTP, which represents the relative location of Switch I; the latter is defined by the distance between the oxygen (OH) atom of Tyr64 and the phosphorus (PG) atom of GTP, which represents the relative location of Switch II. Figure 1 then illustrates the distribution of a number of available X-ray Ras structures on the $dY$-$dT$ plane, which is called $dY$-$dT$ plot. In this plot we find several characteristic structures for State 1 and State 2: For example, the PDB entry 5B30 is a characteristic structure for State 1 with an open conformation between the two switch regions (open form). On the other hand, the PDB entry 5B2Z is a characteristic structure for State 2 in a closed conformation of Switch I, II. These characteristic structures of State 1 and State 2 are distributed over the upper-right and lower-left regions in the $dY$-$dT$ plane, respectively. In addition, we observe intermediate structures such as i61a, originally determined by us (see Supplementary data) but not registered in Protein Data Bank (PDB), and the PDB entry 1LF0, which is a structure of A59G mutant, in the upper-left and lower-right regions, respectively.

Employing some typical X-ray structures from these collections, we have performed molecular dynamics (MD) simulations for Ras proteins with GTP in aqueous solution by the Amber12 and Amber14 softwares [33]. After the addition of missing hydrogen atoms in the PDB structure, the system is solvated by explicit water molecules with crystallized $Mg^{2+}$, hydration waters and some counter ions ($Na^{+}$) to electrically neutralize the unit cell of system under the periodic boundary condition.

*2.2. Molecular dynamics (MD) simulation*

The MD simulations for the solvated Ras systems were carried out with the force fields of ff12SB (from State 1 to State 2) or ff14SB (from State 2 to State 1) for Ras with ions, TIP3P for water, and the Manchester force field [34] for GTP, which was substituted for GppNHp in experiments (see Sec. 3.1 below). Periodic boundary condition was imposed on the rectangular unit cells, in which the thickness of solvated water is more than 12 Å and totally 31261-31792 atoms are contained. After relevant relaxation and heating processes, the NPT simulations with the pressure of 1 atm and the temperature of 300 K were performed, where the Berendsen method [35] with $\tau = 2.0$ ps was employed for the pressure and temperature controls.

Considering that the transitions between State 1 and State 2 would occur at the time scales longer than milli-seconds [6, 8, 10], it is formidable to generate the state transitions of Ras proteins within the framework of conventional MD simulations. Thus, we employed the Parallel Cascade Selection MD (PaCS-MD) [16] to accelerate the approach to the target structure in the present study. Setting the reactant state (initial structure) and the product state (target structure), the PaCS-MD performs multiple independent MD runs in parallel starting with an initial structure in which atoms are given randomized velocities according to the Maxwell-Boltzmann distribution. With the parallel number $N_{parallel}$ ($N_{parallel} = 5$ in the present study) and the MD steps $N_{step}$, we obtain $N_{parallel} \times N_{step}$ snapshots after the first-round MD. Then, selecting a new set of $N_{parallel}$ structures according to the "ranking measure" to judge the similarity to the target structure, we run the next parallelized MD round iteratively with the parallel number $N_{parallel}$ and the

MD steps $N_{step}$. As for the ranking measure, the present work employed the root-mean-square deviation (RMSD) from the target structure, in which the amino-acid residues 32-38 and 59-67 were used for the RMSD calculations. Repeating these MD cycles, we expect that the Ras structure would efficiently change to approach the target structure.

### *2.3. State-transition-based local network entropy (SNE)*

State-transition-based local network entropy (SNE) is defined as an information entropy associated with the critical transition of system and can identify the transition state in leading dynamical networks in terms of an early-warning signal [17, 18]. For instance, concerning a sudden health deterioration during gradual progression of many chronic diseases, a critical phenomenon generally takes place as a drastic transition in the focal system or network from a normal state to a disease state, which corresponds to a bifurcation point in dynamical systems theory [36]. The SNE for leading biomolecular networks then provides a useful tool for quantitatively describing these critical phenomena in disease development and progression. For mathematical modelling, let us consider three states, normal state, pre-disease state and disease state, for state transition. The normal state has a high resistance and robustness against perturbations. The pre-disease state is defined as a limiting state from the normal state just before or at the critical point, and has lower resistance and robustness due to dynamical transition; the system is very sensitive to external stimuli and ready to go to the disease state or go back to the normal state by small perturbations. The disease state is, on the other hand, in the heavily deteriorated stage, which has a high resistance and robustness and is much more difficult to come back to

the normal state by medical treatments than the pre-disease state. The SNE is related with the robustness of network system, which is high in the normal state, drastically decreases in the pre-disease state, and again becomes high in the disease state. One can thus identify the transition state by observing the temporal variations of SNE. Besides, one can address the change of SNE around each central node in addition to that for the whole network, since the SNE can be calculated for each first-order linked network centered at a specified node $i$. Thus we can investigate which nodes are involved in the state transition and to what extent they are.

In the present study, we regard the hydrogen bond in the solvated Ras protein system containing ions, ligand and surrounding water molecules as a node in the network, where the hydrogen bond network associated with functionally important water of hydration is especially focused on. We have calculated the SNE for this system, in which three states, state A (A = 1 or 2), critical (transition) state and state B (B = 2 or 1), are considered corresponding to the normal state, the pre-disease state and the disease state in the mathematical modelling above, respectively.

The SNE is evaluated in this study as follows. Let us define a network with $n$ nodes whose dynamics is described in terms of the Markov process. The state of network at time $t$ is represented by $Z(t) = (z_1, z_2, ..., z_n)$, where $z_j$ refers to a value associated with node $j$ $(1 \leq j \leq n)$. To measure the temporal variation of the state of node $j$, another variable, $x_j(t) \in \{0, 1\}$, is also introduced. At time $t$, if $|z_j(t) - z_j(t - \Delta t)| \geq d_j$ with a threshold value $d_j$, we take $x_j(t) = 1$ and otherwise $x_j(t) = 0$, where $\Delta t$ is a time interval. Thus, $X(t) = (x_1, x_2, ..., x_n)$ represents a transition dynamics of

the network at time $t$. The SNE is then calculated for each local network centered at a node $i$. Let us assume that the node $i$ has $m$ first-order linked nodes, $i_1, ..., i_m$ $(m < n)$, thus forming a local network with time-dependent state $X^i(t) = (x_i, x_{i_1}, ..., x_{i_m})$ centered at node $i$. Since each node has a value $x_j(t) \in \{0, 1\}$, $X^i(t)$ can take $2^{m+1}$ states. We then express the possible states of $X^i(t)$ and $X^i(t+\Delta t)$ as $\{A_v\}_{v=1,2,...,2^{m+1}}$ and $\{A_u\}_{u=1,2,...,2^{m+1}}$, respectively.

The Markov matrix $P = (p_{u,v})$ to represent the transition probability from the state $v$ to the state $u$ of the local network centered at node $i$ is written as

$$p_{u,v}(t) = Pr(X^i(t + \Delta t) = A_u | X^i(t) = A_v), \tag{1}$$

where $u, v \in \{1, 2, ..., 2^{m+1}\}$, $\sum_u p_{u,v}(t) = 1$ and $Pr(\ |\ )$ refers to the conditional probability. Using this Markov matrix, the local SNE for central node $i$ can be obtained as

$$H_i(t) = -\sum_{u,v} \pi_v(t) p_{u,v}(t) \log_2 p_{u,v}(t), \tag{2}$$

where $\pi_v(t) = (\pi_1(t), ..., \pi_{2^{m+1}}(t))$ is a stationary distribution to satisfy $\sum_v \pi_v p_{u,v} = \pi_u$. Further, the total SNE averaged over the whole network with $n$ central nodes is given by

$$H(t) = \frac{1}{n} \sum_{i=1}^{n} H_i(t). \tag{3}$$

The SNE defined above is a kind of conditional entropy and has a correlation with the robustness of network [17, 18]. It thus measures the structural stability and robustness of system in a quantitative way, and can detect the

critical state. In the actual applications, a relevant value is taken for the time interval $\Delta t$, and the probabilities $p_{u,v}(t)$ and $\pi_v(t)$ are evaluated via the temporal average around the time $t$. In the case of solvated Ras system, possible sites for hydrogen bond as nodes are chosen in advance according to stationary molecular configuration near the transition state. If there is a hydrogen bond at the site $j$ at time $t$, we assign $z_j(t) = 1$, and otherwise $z_j(t) = 0$. $x_j(t)$ is then calculated with the threshold value $d_j = 1$. The first-order linked nodes around the central node $i$ are selected on the basis of the mutual information representing the correlation between two nodes [37]:

$$I(A;B) = \tilde{H}(A) - \tilde{H}(A|B). \tag{4}$$

Here, $\tilde{H}(A)$ and $\tilde{H}(A|B)$ refer to the information entropy for event $A = \{a_j\}$ and the conditional entropy for event $A$ given event $B = \{b_k\}$, respectively:

$$\tilde{H}(A) = -\sum_j p(a_j) \log_2 p(a_j), \tag{5}$$

$$\tilde{H}(A|B) = -\sum_j \sum_k p(b_k) p(a_j|b_k) \log_2 p(a_j|b_k), \tag{6}$$

where $p$ refers to the probability for each event.

For the events $A$ and $B$, we consider whether there is a hydrogen bond at that site or not. $\tilde{H}(A)$, $\tilde{H}(A|B)$ and $I(A;B)$ are evaluated by means of averages over MD trajectories, and when the mutual information exceeds a threshold value, we assign a first-order linkage between the two nodes with the events (*i.e.*, formation of hydrogen bond) $A$ and $B$, thus forming a local network around the central node $i$.

## 3. Numerical results and discussion

### *3.1. State transition*

We have performed three types of PaCS-MD simulations to elucidate the molecular mechanism of state transition in Ras/GTP system.

First, we carried out a PaCS-MD simulation in which State 1 (PDB entry: 5B30) and State 2 (PDB entry: 5B2Z) were chosen as the initial and target structures, respectively. We have thus obtained a trajectory A with 905 cycles of PaCS-MD for 5099 ps, and Fig. 2 shows in $dY$-$dT$ plot that the final state is trapped before reaching the target structure. Figure 3 then illustrates a comparison of the initial, final and target structures observed in trajectory A, showing that the final structure actually lies between the initial and target structures; the final structure is nearly approaching the target structure in Switch II region, while the side chain of Thr35 in Switch I still remains near the initial structure and is not oriented toward $Mg^{2+}$ as expected in State 2. We can thus regard this final structure as a kind of "intermediate state (structure)" between State 1 and State 2. Figure 2 indicates that the $dY$ value associated with Switch II decreases below 12 Å, while the $dT$ value associated with Switch I remains around 9 Å. To elucidate the reason why Switch I was not fully closed, we have performed the structural analysis in more detail and found that the movement of the side chain of Thr35 in Switch I was restricted since Switch II got closed in advance. Figure 3(d) illustrates the interference of motions between Thr35 and Tyr64.

Next, in order to suppress the over-closing of Switch II, we have performed a PaCS-MD simulation from State 1 to State 2, in which the target structures were set at two stages; that is, an intermediate state (i61a) was employed

as the first target, and then State 2 (5B2Z) was taken as the second (final) target. The crystal structure of i61a was determined using the diffraction data collected at ambient temperature as shown in Supplementary data. We have thus obtained a trajectory B for 4053 ps, which is illustrated in $dY$-$dT$ plot of Fig. 2. The superposition of the initial, final and (second) target structures is depicted in Fig. 4, showing that both the Switch I, II were nearly closed in the final structure, where the side chain of Thr35 in Switch I was directed toward $Mg^{2+}$ as in State 2. Figure 2 shows that the $dY$ and $dT$ values of the final state were less than 12 Å and 7 Å, respectively; the decrease in $dY$ was suppressed before the $dT$ value decreased below 8 Å, indicating that Switch II did not restrict the motion of the side chain of Thr35. In addition to Thr35, there is a significant difference between State 1 and State 2 concerning the structure of side chain of Tyr32 [10]. Comparing the trajectories A and B, we have found a marked difference in the distance between Tyr32 (HH atom) and GTP (O1G atom), as shown in Fig. 5(a). In the case of trajectory B, the hydrogen bond between Tyr32 and GTP was broken by the insertion of a hydration water (WAT246), as seen in Fig. 4(d). The hydrogen bond between Tyr32 and GTP plays an important role to suppress the fluctuation in Switch I, thus inhibiting the structural transition from State 1 to State 2. Calculating the RMSDs compared to State 2, we have found in Fig. 5 (b) and (c) that the movements of Pro34, Glu63 and Tyr64 were triggered by the movement of Tyr32 at no later than 1000 ps. We have also observed that the motions of Asp33, Pro34, Thr35, Ile36 and Glu37 were well correlated with that of Switch I, whereas the motions of Glu63 and Tyr64 were well correlated with that of Switch II, thus providing

relevant indicators for describing the motions of the two switches.

Third, we have studied the transition from State 2 to State 1 in comparison with experimental results [10]. When we performed a PaCS-MD simulation starting with State 2 (5B2Z) toward the target structure of State 1 (5B30), we found a trajectory C with 40 cycles for 767 ps in $dY$-$dT$ plot depicted in Fig. 6(a). We then see in Fig. 7 that Thr35 in Switch I did not move so much with retaining a bond to $Mg^{2+}$, while the side chain of Tyr64 in Switch II got oriented to the target structure of State 1, thus showing that the Switch II region is easy to fluctuate toward the structural transition. Since Fig. 6(a) shows that the $dT$ value in the trajectory C did not change due to the strong bonding between Thr35 and $Mg^{2+}$, we then modified the ranking measure in PaCS-MD so that the RMSD for all atoms of Switch regions including the side chains was used (ranking measure A) for 1-400 cycles (1-2626 ps) and that excluding the side chains was employed (ranking measure B) for 401-600 cycles (2623-4531 ps) in order to release the constraint on the side chains. However, as seen in Fig. 6 (b) and (c) for this trajectory C2, the increase of $dT$ value was not observed still, again indicating that the Switch I region in the closed conformation is very stable.

We have then compared the structural changes observed in trajectory C2 with a transition model suggested through experimental observations [10]. According to a scenario proposed by Matsumoto *et al.* [10], the state transition from State 2 to State 1 would take place as follows: First, the side chain of Gln61 moves toward Arg68 and makes a hydrogen bond to the main chain of Glu63. Then the hydrogen bonds are also formed between Gln61 and Gln99, and between Gln 61 and Tyr96. Owing to the orientational change

of Gln61, the side chain of Arg68 approaches the main chain of Gly60, thus forming a hydrogen bond. Spurred by these structural changes in the Switch II region, the bonding between Tyr32 in Switch I and GTP is weakened and Tyr32 moves toward Pro34. The breakage of the bonding between Thr35 and the $\gamma$-phosphate of GTP is then caused, finally leading to the transition of Switch I to the State 1 configuration. In the trajectory C2 obtained by PaCS-MD simulation, the side chain of Gln61 actually moves toward Arg68 (Fig. 8(a)) as in the scenario above. However, Arg68 moves away from Gly60 rather than approaching, thus bringing about a relative orientation among these residues different from the experimental model above. Fig. 8(b) shows the side chain of Gln61 is approaching the main chain of Glu63, giving a relative location consistent with the experimental observation. Fig. 8(c) indicates that the relative location between Gln61 and Tyr96 is also consistent with the above model, but that between Gln61 and Gln99 is an unexpected one associated with the relative positions of Gln61 and Arg68. If the positions of Gln61 and Arg68 would be exchanged, the distance between Gln61 and Gln99 would become shorter, as expected in the scenario above. Concerning the structural changes in the Switch I region, on the other hand, it is observed in the trajectory C2 that the side chain of Tyr32 is moving toward Pro34. This is consistent with the experimental finding [10], while it does not cause the breakage of the bond between Thr35 and GTP or $Mg^{2+}$, as seen in Fig. 8(d). Figure 9 illustrates the temporal evolutions of the distances between key residues to see how the structural changes in the Switch II region actually occurred in trajectory C2: Q61(OE1)-R68(HH11), Q61(OE1)-E63(H), Q61(H)-Y96(OH) and Q61(HE21)-Q99(OE1), where the characters in the

parentheses refer to the atom names in PDB. This figure shows that there was an order of occurrence in the structural changes observed in trajectory C2: First, the distances of Gln61-Arg68 and Gln61-Gln99 decreased, and subsequently that of Gln61-Tyr96 did. Since Gln61 made a hydrogen bond with Arg68 in trajectory C2, the side chain of Gln61 could not make a hydrogen bond with the main chain of Glu63. This hydrogen bond between Gln61 and Arg68 seems to make the interchange of their side chains difficult, thus causing their relative locations different from the experimental scenario. However, the simulation results observed in trajectory C2 were consistent with the experimental model in that Gln61 moved toward Arg68 and the main chain of Gln61 and the side chain of Tyr96 made a hydrogen bond. In passing, it is also noted that the GTP ligand was employed in the present simulation study in contrast to GppNHp employed in the experiments [10]. It is known [1, 38] that the use of GTP would make the closed conformation of switches more stable, somewhat tending to favor State 2 compared to the GppNHp case.

We see in the above analysis that the solid bonding of Thr35 with GTP or $Mg^{2+}$ makes the transition to State 1 difficult. Since it is experimentally known [6, 10, 38, 39] that the fraction of State 1 increases in T35S mutants, we have also carried out a PaCS-MD simulation for T35S mutant starting with the State 2 structure, where T35S mutant was constructed from the wild-type (WT) structure of State 2 (5B2Z) and the HB2 atom of Ser35 was used in place of the OG1 atom of Thr35 for the evaluation of $dT$ value. The calculated trajectory D with 200 cycles for 1259 ps is illustrated in $dY$-$dT$ plot in Fig. 6(a), again indicating that Switch I did not open; the structural

analysis then shows that the substituted Ser35 still retained the bonding with $Mg^{2+}$, thus stabilizing the Switch I region. Detailed analysis has also shown that the hydrogen bond between Gln61 and Arg68 as seen in the trajectory C2 is not observed in the trajectory D, which is a marked difference from the trajectry C2 that may enable the exchange of locations between Gln61 and Arg68.

It is also known [38, 39] that almost all T35A mutants take the State 1 structure rather than the State 2 structure. We have then performed a PaCS-MD simulation for T35A mutant constructed from the WT structure of State 2 (5B2Z), where the HB2 atom of Ala35 was used in place of the OG1 atom of Thr35 for the evaluation of $dT$ value. Through 600 cycle (3446 ps) PaCS-MD targeting to State 1, trajectory E, shown in Fig. 6(a), has been obtained. It has been observed in this simulation that both the Switch I, II approached the structures in State 1 (see Fig. 10). It is characteristic that the orientation of Ala35 significantly changed toward the target structure of State 1, in which the missing bond between Ala35 and $Mg^{2+}$ caused the structural change of Switch I. As observed in Fig. 6(a) for trajectory E, both the $dY$ and $dT$ values increased simultaneously in the state transition. Detailed structural analysis has shown that Gln61 moved to the location of Arg68 and accordingly Gln61 approached Glu63 (see Fig. 10 (d) and (e)). Gln61 also approached Gln99, whereas Gln99 moved toward a direction somewhat away from Gln61, thus not forming a hydrogen bond between them (Fig. 10(f)). Gln61 and Tyr96, on the other hand, approached each other, as suggested in the experimental scenario [10]. Switch I moved significantly in the trajectory E as seen in Fig. 10(g), where the side chain of Tyr32 moved to the

initial location of Pro34 in agreement with the experimental suggestion [10]. Figure 11 illustrates the temporal evolutions of the distances between some key residues: Q61(NE2)-R68(HB3), Q61(OE1)-E63(H), Q61(H)-Y96(OH), Q61(HE21)-Q99(OE1), A35(HB2)-GTP(O2G) and Y32(HD2)-P34(HG3), where the characters in the parentheses refer to the atom names in PDB. This figure shows that the formation of hydrogen bond between Gln61 and Tyr96 took place prior to that between Gln61 and Arg68 (and Glu63). The fluctuations in the Switch II region in the trajectory E were larger than those in the trajectories C2 and D, which is also verified by Fig. 6(a). Concerning the structural change in the Switch I region, the bond between Ala35 and GTP was broken before Tyr32 approached Pro34 in the case of T35A mutant. This suggests that the reason for the opening of Switch I in T35A mutant should not be attributed to the motion of Tyr32 but to the breakage of the bond between Ala35 and $Mg^{2+}$.

### *3.2. Temporal variations of SNE associated with hydrogen bond network*

In this subsection we perform the SNE analysis on the hydrogen bond network related to the state transition of Ras protein. Before performing the SNE analysis, we have investigated the hydration water molecules surrounding the Ras protein and detected seven water molecules that are immobile and should be important for the state transition (see Table 1 and Fig. 12). We have then specified a hydrogen bond (HB) network composed of these (immobile) seven water molecules, GTP, $Mg^{2+}$ and 13 residues of Ras protein, which is depicted in Fig. 13. In this network we have identified 15 possible sites for HB formation around the State 1 (5B30) structure of H-Ras. Employing the 4053 ps PaCS-MD trajectory B from State 1 to State 2

(see Fig. 2), we have then calculated the connection probability of fluctuating HB at each site, where the presence of HB is defined by the criterion that the distance between the pertinent two atoms is within 2.5 Å. These connection probabilities for the 15 HB sites are listed in Table 2: HB is formed with the probability beyond 0.95 for the sites 1, 4, 6, 7, 10-15 in which very immobile water molecules $W_{172}, W_{173}, W_{177}$ and $W_{180}$ are involved. Other HB sites, $2, 3, 5, 8$ and 9, have the connection probabilities less than 0.95, which are associated with $W_{191}$, $W_{207}$ and GTP, thus indicating the temporal variations of HB formation. It is especially noted that the HB sites of 2, 3 and 5 are susceptible to structural fluctuations.

We have next calculated the mutual information (MI) for any pair of the 15 HB sites. Dividing the trajectory B into the intervals of 100 ps, we evaluated the MI due to Eq. (4) using the HB formation probabilities during these periods. Figure 14(a) illustrates the time-dependent MI which exceeded 0.1 at any time interval. As observed in Fig. 14(a), there are 17 pairs of HB sites whose MI exceeded 0.1 at any interval, thus showing the inter-dependency or correlation in the HB network. It is noted that the MIs associated with the HB sites of 1 and 6 took zero values because the HB connection probabilities of these HB sites were 1.0 throughout the trajectory B. It is also seen in Fig. 14(a) that the peak positions of MI of HB pairs are distributed temporally, which indicates that the information transmission concerning the HB-related state transition is not taking place simultaneously, but gradually occurs step by step; the peaks associated with the HB sites near Switch I (2, 3 and 5) and Switch II (7, 8 and 9) are observed over time. Figure 14 (b) and (c) then show the variations of MI as functions of $dY$ and

$dT$, respectively, where it is noted that both $dY$ and $dT$ values decrease as the transition from State 1 to State 2 proceeds. It is observed in Fig. 14(b) for $dY$ that the HB sites of 3, 5, 9 and 15 are mainly involved and play important roles for the closing of Switch II. Initially, the MIs for 2-13 and 9-13 pairs show high values at around $dY$ = 21-22 Å, indicating that the strong (correlated) dependence on the HB site 13 changes from the site 2 to the site 9 which are located nearly each other (see Fig. 13). Further, 3-9, 3-8 and 8-9 pairs take high MI values as $dY$ decreases from 17 Å to 15 Å, thus indicating that the strong dependence on the site 3 changes from the site 9 to the site 8 that is located more closely to Switch II. On the other hand, Fig. 14(c) for $dT$ shows that there are a number of correlated pairs containing the HB sites of 2 and 3 when $dT$ decreases from 13 Å to 11 Å. It is noted that the HB of site 2 is a vulnerable bonding between Switch I and GTP (see Table 2) and therefore plays a key role for the closing of Switch I. The MI for the pair of sites 2 and 3 is high at $dT$ = 13 Å, while the MIs of the site 2 or 3 are high with other sites for $dT$ = 11-12 Å, which indicates that both HB sites of 2 and 3 play important roles to transmit the information associated with the motion of Switch I over a wide region of HB network. Table 3 lists the HB pairs whose MI exceeded 0.4 at any time or any value of $dY$ or $dT$, which are regarded as forming local, connected HB networks (simple graphs) centered at a designated HB site (central node). In this table the local HB networks centered at the sites 1 and 6 are not shown because these two sites form the firm HB with the probability 1.0 throughout the PaCS-MD simulation for the trajectory B.

Before performing the SNE analysis for the trajectory B, we calculated

the temporal evolution of SNEs by employing the trajectory A in which the state transition from State 1 to State 2 was not complete (see Fig. 2). In the SNE calculations, the stationary probability $\pi_v(t)$ and the transition probability $p_{u,v}(t)$ were evaluated with the sampling period of 500 ps around the time $t$ and the transition time interval $\Delta t = 3$ ps, which led to sharp changes of calculated SNEs. Figure 15(a) illustrates the temporal evolution of the SNEs for each local network centered at designated nodes and their average over the whole network. We thus observe significant decreases in the SNE values associated with some central nodes, indicating an emergence of state transition. However, the recovery (increase) of SNEs toward the higher values, which represents the transition to another state, was not clearly found in this case for the trajectory A due to the cease of state transition, as seen in Fig. 2.

We next carried out the SNE calculations employing the trajectory B, in which the same sampling period of 500 ps around the time $t$ and the same transition time interval $\Delta t = 3$ ps were used as in the case of trajectory A. Figure 15(b) shows the temporal evolution of SNEs, indicating their decreases in the yellow domain (1.75-2.75 ns) associated with the state transition. It is remarkable that some SNEs steeply decrease and then increase, thus showing the presence of the critical (transition) state. It is also found that the local networks for almost all the central nodes except for the site 2 are involved in this state transition. It is remarked here that the site 2 of HB between Tyr32 and GTP was broken at no later than 1 ns, as seen in Fig. 5, which triggered the state transition. We further performed the SNE calculation for the trajectory B in which the sampling time of 100 ps was employed to

detect sharper temporal changes. Observing Fig. 15(c) for this calculated result, one can see that the sites 3 and 12 are key indicators for the state transition. It is noted that the water molecules $W_{207}$ and $W_{180}$ associated with the HB sites 3 and 12, respectively, have been regarded as key waters in the preceding studies [12] and the analysis above. Moreover, in addition to the HB sites 3 and 12, we see in Fig. 15(c) the importance of HB sites 14, 15, 4, 7, 9, 8 and 11 in this order.

Further, to see the relationship between the temporal variation of SNE and the structural change of Ras, we plot the trajectory B on the $dY$-$dT$ plane in Fig. 16(a) (see also Fig. 2), in which the points at $t = 2.5$, 2.7 and 2.9 ns are marked. This figure shows that Switch II first closes partially, Switch I next closes, and finally Switch II closes fully. In the time region of 2.0-2.6 ns, we observe that Switch II opened slightly to make Switch I close by relaxing the steric hindrance between the two switches. After Switch I had closed fully, Switch II closed completely, as seen for the location of three points depicted in Fig. 16(a). The SNE decreased when Switch I closed and Switch II slightly opened, and it then increased when Switch II closed. Figure 16 (b) and (c) illustrate the snapshots of Ras at $t = 2.5$, 2.7 and 2.9 ns, in which Thr35 was approaching GTP, while Tyr64 was first getting away from GTP and next approaching it; these dynamical behaviors of Tyr64 coincided with the temporal variation of SNE mentioned above.

## 4. Conclusions

In the present study we have analyzed the state transition of solvated H-Ras/GTP system in terms of PaCS-MD simulations. By accelerating the

structural changes of Ras protein between inactive State 1 and active State 2, which are associated with the motions of the two switch regions, we have elucidated the molecular mechanisms of the state transitions in atomic details. These computational results have then been compared to the molecular model proposed through experimental observations [10], leading to fairly consistent pictures for the state transition along with some minor differences between the both results, which may be partially attributed to the use of GTP instead of GppNHp employed in the experiments. In order to find more useful information to design the effective inhibitors targeting the cancer-related Ras proteins, the improvements in the MD protocols with higher efficiencies and accuracies would be required in conjunction with extensive interpolations of experimentally available snapshot structures of Ras proteins.

In addition to the direct observation of the structural changes in Ras proteins, we have also proposed a novel approach in this study to detecting the state transition in terms of the dynamical information entropy SNE associated with the hydrogen bond network mainly composed of surrounding water molecules. It is known [40–42] that solvation waters surrounding biomolecules significantly contribute to thermodynamics of the whole molecular systems. The dynamical change of the entropy [43] associated with hydration water is thus expected to become a good indicator for representing the thermodynamic stabilities of solvated biomolecular systems. The present study, to the best of our knowledge, has provided a first example to show that the dynamical behaviors of (information) entropy of surrounding water can describe the state transition of hydrated biomolecules in a quantitative manner, thus opening a new avenue of theoretical analysis.

## Acknowledgements

We would like to acknowledge the Grants-in-Aid for Scientific Research (No. 26460035, 26293026 and 26293065) from the Japan Society for the Promotion of Science.

## Supplementary data

Supplementary data associated with this article can be found in the online version.

## References


[1] M. Geyer, T. Schweins, C. Herrmann, T. Prisner, A. Wittinghofer, H.R. Kalbitzer, Conformational transitions in p21ras and in its complexes with the effector protein Raf-RBD and the GTPase activating protein GAP, Biochemistry. 35 (1996) 10308-20.

[2] K. Scheffzek, M.R. Ahmadian, W. Kabsch, L. Wiesmüller, A. Lautwein, F. Schmitz, A. Wittinghofer, The Ras-RasGAP complex: structural basis for GTPase activation and its loss in oncogenic Ras mutants, Science 277 (1997) 333-338.

[3] P.A. Boriack-Sjodin, S.M. Margarit, D. Bar-Sagi, J. Kuriyan, The structural basis of the activation of Ras by Sos, Nature 394 (1998) 337-343.

[4] M. Malumbres, M. Barbacid, RAS oncogenes: the first 30 years, Nat. Rev. Cancer. 3 (2003) 459-465.

[5] A.E. Karnoub, R.A. Weinberg, Ras oncogenes: split personalities, Nat. Rev. Mol. Cell Biol. 9 (2008) 517-531.

[6] F. Shima, Y. Ijiri, S. Muraoka, J. Liao, M. Ye, M. Araki, K. Matsumoto, N. Yamamoto, T. Sugimoto, Y. Yoshikawa, T. Kumasaka, M. Yamamoto, A. Tamura, T. Kataoka, Structural basis for conformational dynamics of GTP-bound ras protein, J. Biol. Chem. 285 (2010) 22696-22705.

[7] M. Araki, F. Shima, Y. Yoshikawa, S. Muraoka, Y. Ijiri, Y. Nagahara, T. Shirono, T. Kataoka, A. Tamura, Solution structure of the state 1

conformer of GTP-bound H-Ras protein and distinct dynamic properties between the state 1 and state 2 conformers, J. Biol. Chem. 286 (2011) 39644-53.

[8] F. Shima, Y. Yoshikawa, M. Ye, M. Araki, S. Matsumoto, J. Liao, L. Hu, T. Sugimoto, Y. Ijiri, a Takeda, Y. Nishiyama, C. Sato, S. Muraoka, a Tamura, T. Osoda, K. Tsuda, T. Miyakawa, H. Fukunishi, J. Shimada, T. Kumasaka, M. Yamamoto, T. Kataoka, In silico discovery of small-molecule Ras inhibitors that display antitumor activity by blocking the Ras-effector interaction, Proc Natl Acad Sci U S A. 110 (2013) 8182-8187.

[9] R. Knihtila, G. Holzapfel, K. Weiss, F. Meilleur, C. Mattos, Neutron crystal structure of RAS GTPase puts in question the protonation state of the GTP $\gamma$-phosphate, J. Biol. Chem. 290 (2015) 31025-31036.

[10] S. Matsumoto, N. Miyano, S. Baba, J. Liao, T. Kawamura, C. Tsuda, A. Takeda, M. Yamamoto, T. Kumasaka, T. Kataoka, F. Shima, Molecular mechanism for conformational dynamics of Ras · GTP elucidated from in-situ structural transition in crystal, Sci. Rep. 6 (2016) 1-12.

[11] C. Kobayashi, S. Saito, Relation between the conformational heterogeneity and reaction cycle of Ras: Molecular simulation of Ras, Biophys. J. 99 (2010) 3726-3734.

[12] P. Prakash, A. Sayyed-Ahmad, A.A. Gorfe, The role of conserved waters in conformational transitions of Q61H K-ras, PLoS Comput. Biol. 8 (2012) 1-11.

[13] T. Miyakawa, R. Morikawa, M. Takasu, K. Sugimori, T. Mizukami, K. Kawaguchi, H. Saito, H. Nagao, Molecular dynamics simulations of the Hras-GTP complex and the Hras-GDP complex, Int. J. Quantum Chem. 113 (2013) 2333-2337.

[14] T. Miyakawa, R. Morikawa, M. Takasu, K. Sugimori, K. Kawaguchi, H. Saito, H. Nagao, Analysis of water molecules around GTP in Hras-GTP complex and GDP in Hras-GDP complex by molecular dynamics simulations, Mol. Phys. 112 (2014) 526-532.

[15] N. Sharma, U. Sonavane, R. Joshi, Probing the wild-type HRas activation mechanism using steered molecular dynamics, understanding the energy barrier and role of water in the activation, Eur. Biophys. J. 43 (2014) 81-95.

[16] R. Harada, A. Kitao, Parallel cascade selection molecular dynamics (PaCS-MD) to generate conformational transition pathway, J. Chem. Phys. 139 (2013) 1-10.

[17] L. Chen, R. Liu, Z.-P. Liu, M. Li, K. Aihara, Detecting early-warning signals for sudden deterioration of complex diseases by dynamical network biomarkers, Sci. Rep. 2 (2012) 18-20.

[18] R. Liu, M. Li, Z.-P. Liu, J. Wu, L. Chen, K. Aihara, Identifying critical transitions and their leading biomolecular networks in complex diseases, Sci. Rep. 2 (2012) 1-9.

[19] A. Achiron, I. Grotto, R. Balicer, D. Magalashvili, A. Feldman, M. Gurevich, Microarray analysis identifies altered regulation of nuclear

receptor family members in the pre-disease state of multiple sclerosis, Neurobiol. Dis. 38 (2010) 201-209.

[20] L. Chen, R. Wang, C. Li, K. Aihara, Modeling biomolecular networks in cells: Structures and dynamics, Springer (2010).

[21] P. Chen, R. Liu, Y. Li, L. Chen, Detecting critical state before phase transition of complex biological systems by hidden Markov model, Bioinformatics 32 (2016) 2143-2150.

[22] R. Donangelo, H. Fort, V. Dakos, M. Scheffer, and E. H. Van Nes, Early warnings for catastrophic shifts in ecosystems: comparison between spatial and temporal indicators, Int. J. Bifurc. Chaos 20 (2010) 315-321.

[23] S. R. Carpenter, J. Cole, M. L. Pace, R. Batt, W. A. Brock, and T. Cline, J. Coloso, J.R. Hodgson, J.F. Kitchell, D.A. Seekell, L. Smith, B. Weidel, Early warnings of regime shifts: a whole-ecosystem experiment, Science 332 (2011) 1076-1079.

[24] S. R. Carpenter, W. A. Brock, Rising variance: a leading indicator of ecological transition, Ecol. Lett. 9 (2006) 308-315.

[25] V. Guttal, C. Jayaprakash, Changing skewness: an early warning signal of regime shifts in ecosystems, Ecol. Lett. 11 (2008) 450-460.

[26] M. Li, T. Zeng, R. Liu, L. Chen, Detecting tissue-specific early warning signals for complex diseases based on dynamical network biomarkers: study of type 2 diabetes by cross-tissue analysis, Brief. Bioinform. 15 (2013) 229-243.

[27] R. Liu, P. Chen, K. Aihara, L. Chen, Identifying early-warning signals of critical transitions with strong noise by dynamical network markers, Sci. Rep. 5 (2015) 1-13.

[28] R. Liu, X. Yu, X. Liu, D. Xu, K. Aihara, L. Chen, Identifying critical transitions of complex diseases based on a single sample, Bioinformatics 30 (2014) 1579-1586.

[29] L. Chen, R.-S. Wang, X.-S. Zhang, Biomolecular networks, Wiley (2009).

[30] R. Pastor-barriuso, E. Guallar, J. Coresh, Transition models for change-point estimation in logistic regression, Stat. Med. 22 (2003) 1141-1162.

[31] M. Scheffer, J. Bascompte, W.A. Brock, V. Brovkin, S.R. Carpenter, V. Dakos, H. Held, E.H. Van Nes, M. Rietkerk, G. Sugihara, Early-warning signals for critical transitions, Nature 461 (2009) 53-59.

[32] G. Tanaka, K. Tsumoto, S. Tsuji, K. Aihara, Bifurcation analysis on a hybrid systems model of intermittent hormonal therapy for prostate cancer, Phys. D Nonlinear Phenom. 237 (2008) 2616-2627.

[33] D.A. Pearlman, D.A. Case, J.W. Caldwell, W.S. Ross, T.E. Cheatham, S. DeBolt, D. Ferguson, G. Seibel, P.A. Kollman, AMBER, a package of computer programs for applying molecular mechanics, normal mode analysis, molecular dynamics and free energy calculations to simulate the structural and energetic properties of molecules, Comput. Phys. Commun. 91 (1995) 1-41.

[34] K.L. Meagher, L.T. Redman, H.A. Carlson, Development of polyphosphate parameters for use with the AMBER force field, J. Comput. Chem. 24 (2003) 1016-1025.

[35] H.J.C. Berendsen, J.P.M. Postma, W.F. van Gunsteren, A. DiNola, J.R. Haak, Molecular dynamics with coupling to an external bath, J. Chem. Phys. 81 (1984) 3684-3690.

[36] J.D. Murray, Mathematical Biology, Springer (1993).

[37] S. Uda and S. Kuroda, Analysis of cellular signal transduction from an information theoretic approach, Semin. Cell Dev. Biol. 51 (2016) 24-31.

[38] M. Spoerner, A. Nuehs, C. Herrmann, G. Steiner and H.R. Kalbitzer, Slow conformational dynamics of the guanine nucleotide-binding protein Ras complexed with the GTP analogue GTP$\gamma$S, FEBS J. 274 (2007) 1419-1433.

[39] M. Spoerner, C. Herrmann, I.R. Vetter, H.R. Kalbitzer and A. Wittinghofer, Dynamic properties of the Ras switch I region and its importance for binding to effectors, Proc. Natl. Acad. Sci. U.S.A. 98 (2001) 4944-4949.

[40] M. Nakano, H. Tateishi-Karimata, S. Tanaka, F. Tama, O. Miyashita, S. Nakano, N. Sugimoto, Thermodynamic properties of water molecules in the presence of cosolute depend on DNA structure: A study using grid inhomogeneous solvation theory, Nucl. Acids Res. 43 (2015) 10114-10125.

[41] M. Nakano, H. Tateishi-Karimata, S. Tanaka, F. Tama, O. Miyashita, S. Nakano, N. Sugimoto, Local thermodynamics of the water molecules around single- and double-stranded DNA studied by grid inhomogeneous solvation theory, Chem. Phys. Lett. 660 (2016) 250-255.

[42] S. Uehara, S. Tanaka, AutoDock-GIST: Incorporating thermodynamics of active-site water into scoring function for accurate protein-ligand docking, Molecules 21 (2016) 1604.

[43] S. Tanaka, Diffusion Monte Carlo study on temporal evolution of entropy and free energy in nonequilibrium processes, J. Chem. Phys. 144 (2016) 094103.

## Tables and Figures

Table 1. List of immobile hydration water molecules in the structure of State 1 (PDB entry: 5B30) along with the residue ID (see Fig. 12).

| Residue ID | 203 | 213 | 205 | 183 | 182 | 185 | 180 |
|---|---|---|---|---|---|---|---|
| Name | $W_{172}$ | $W_A$ | $W_{207}$ | $W_{173}$ | $W_{191}$ | $W_{180}$ | $W_{177}$ |

Table 2. Connection probabilities of 15 HB sites.

| HB ID | Probability |
|---|---|
| 1 | 1.000 |
| 2 | 0.096 |
| 3 | 0.222 |
| 4 | 0.982 |
| 5 | 0.101 |
| 6 | 1.000 |
| 7 | 0.997 |
| 8 | 0.930 |
| 9 | 0.850 |
| 10 | 0.999 |
| 11 | 0.990 |
| 12 | 0.997 |
| 13 | 0.998 |
| 14 | 0.996 |
| 15 | 0.954 |

Table 3. List of correlated hydrogen bonds except for the sites 1 and 6 whose HB formation probabilities are unity.

| HB ID | Connected sites |
|---|---|
| 2 | 3, 13 |
| 3 | 2, 5, 7, 11, 12, 13 |
| 4 | 5, 8, 10, 11, 12, 15 |
| 5 | 3, 4, 7, 12, 14 |
| 7 | 3, 5, 8, 9, 15 |
| 8 | 4, 7, 9, 10, 11, 13, 15 |
| 9 | 7, 8, 11, 14 |
| 10 | 4, 8, 11, 15 |
| 11 | 3, 4, 8, 9, 10, 15 |
| 12 | 3, 4, 5, 14, 15 |
| 13 | 2, 3, 8, 14 |
| 14 | 5, 9, 12, 13, 15 |
| 15 | 4, 7, 8, 10, 11, 12, 14 |

Figure 1: Classification of X-ray structures of Ras, where each structure is depicted by filled red symbol with Protein Data Bank (PDB) code. The classification is based on the distance ($dT$) between the OG1 atom of Thr35 and PG atom of GTP (GppNHp in experiments), and the distance ($dY$) between the OH atom of Tyr64 and PG atom of GTP (GppNHp in experiments), as shown in the inset. If Ras proteins have GDP instead of GTP, $dT$ and $dY$ are calculated by using the PB atom of GDP instead of the PG atom of GTP. PDB IDs are labeled where space permits. 5B2Z is depicted in blue for clarity, and i61a has no PDB ID.

Figure 2: $dY$-$dT$ plot for trajectory A (blue) and trajectory B (red). Filled black symbols refer to the start or end points of PaCS-MD simulations. Filled red symbols are the same as in Fig. 1.

Figure 3: Comparison of the structures at 1 ps (red), 5099 ps (yellow) of trajectory A and of State 2 (5B2Z, blue). (a) Overall structures, where two switch regions are encircled by dotted lines. (b) and (c) are the close-up views for Switch I and Switch II regions, respectively. (d) Close-up view of the structure around Thr35 and Tyr64, where Thr35 collides with Tyr64.

Figure 4: Comparison of the structures at 1 ps (red), 4053 ps (yellow) of trajectory B and of State 2 (5B2Z, blue). (a) Overall structures, where two switch regions are encircled by dotted lines. (b) and (c) are the close-up views for Switch I and Switch II regions, respectively. (d) Comparison of the hydrogen bond networks around Tyr32 between the structures at 392 ps (left) and 393 ps (right); water molecules (WAT), Tyr32 and GTP are shown in the stick model; $Mg^{2+}$ is shown by a green sphere; hydrogen bonds are represented by orange and cyan lines.

Figure 5: (a) Distance between Tyr32 (HH atom) and GTP (O1G atom); blue line: trajectory A, red line: trajectory B. (b) Temporal evolutions of the RMSDs from the target structure of the residues in Switch I region for trajectory B. (c) Temporal evolutions of the RMSDs from the target structure of the residues in Switch II region for trajectory B.

Figure 6: (a) $dY$-$dT$ plots for the trajectories C (blue), D (red) and E (yellow); filled red symbols are the same as in Fig. 1. (b) $dY$-$dT$ plot for trajectory C2, where the results obtained by using the ranking measure A and B are represented by green and yellow lines, respectively. (c) Enlarged view of (b).

Figure 7: Comparison of the structures at 1 ps (red), 767 ps (yellow) of trajectory C and State 1 (5B30, blue). (a) Overall structures, where two switch regions are encircled by dotted lines. (b) and (c) are the close-up views of Switch I and Switch II regions, respectively.

Figure 8: Comparison of the structures at 1 ps (red) and 4531 ps (yellow) of trajectory C2. Tyr32, Pro34, Thr35, Gln61, Glu63, Arg68, Tyr96 and Gln99 are shown by the stick models. GTP is shown by the line model. (a)-(c): Switch II region. (d): Switch I region.

Figure 9: Temporal evolutions of some indicators for the movement of Switch II region. Q61(HE21)-Q99(OE1) represents the distance between the HE21 atom of Gln61 and the OE1 atom of Gln99. Other indicators are analogous. The vertical line at 2626 ps indicates the borderline between using the ranking measures A and B.

Figure 10: Comparison of the structures at 1 ps (red), 3446 ps (yellow) of trajectory E and of State 1 (5B30, blue). (a) Overall structures, where two switch regions are encircled by dotted lines. (b) and (c) are the close-up views of Switch I and Switch II regions, respectively. In the close-up views of (d)-(g), Tyr32, Pro34, Ala35, Gln61, Glu63, Arg68, Tyr96 and Gln99 are shown by the stick models, and GTP is shown by the line model.

Figure 11: Temporal evolutions of some indicators for trajectory E. The movements of Switch II and Switch I regions are depicted in (a) and (b), respectively. Q61(HE21)-Q99(OE1) means the distance between the atom HE21 of Gln61 and the atom OE1 of Gln99. Other indicators are depicted analogously.

Figure 12: Location of hydration water molecules in the structure of State 1 (5B30) (see Table 1). GTP is shown in the stick model, and $Mg^{2+}$ is shown by a green sphere.

Figure 13: Schematic figure of hydrogen bond (HB) network in State 1 (5B30). 15 numbered dotted orange lines refer to the HB sites. The residues colored in pink and green are located in or near the Switch I and Switch II regions, respectively.

Figure 14: Mutual information of some pairs of hydrogen bonds in the network as functions of (a) time, (b) $dY$, and (c) $dT$.

Figure 15: Temporal evolutions of SNE for each central node in the hydrogen bond network. (a) Trajectory A with sampling time of 500 ps. (b) Trajectory B with sampling time of 500 ps. (c) Trajectory B with sampling time of 100 ps. Yellow domains refer to the transition regions.

Figure 16: (a) Trajectory B and snapshot points at 2500 ps (green), 2700 ps (yellow) and 2900 ps (blue). (b) and (c) show the relative locations of GTP with Thr35 and Tyr64, respectively, where colors correspond to the points in (a).

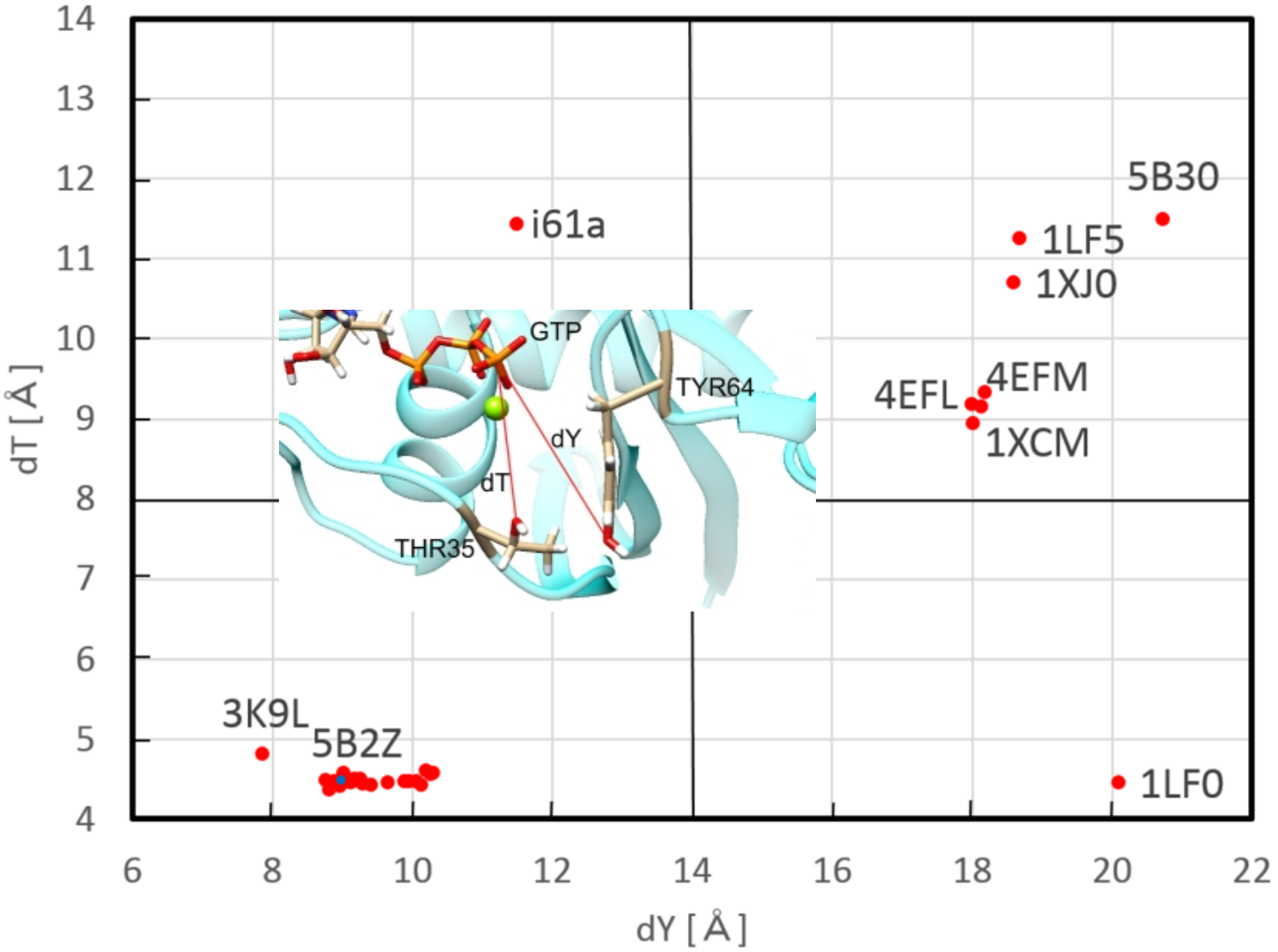
14
13
12
11
10
9
8
7
6
5
4
dT [Å]
6
8
10
12
14
16
18
20
22
dY [Å]
i61a
5B30
1LF5
1XJ0
4EFL
4EFM
1XCM
3K9L
5B2Z
1LF0
GTP
TYR64
dY
dT
THR35

Figure 1

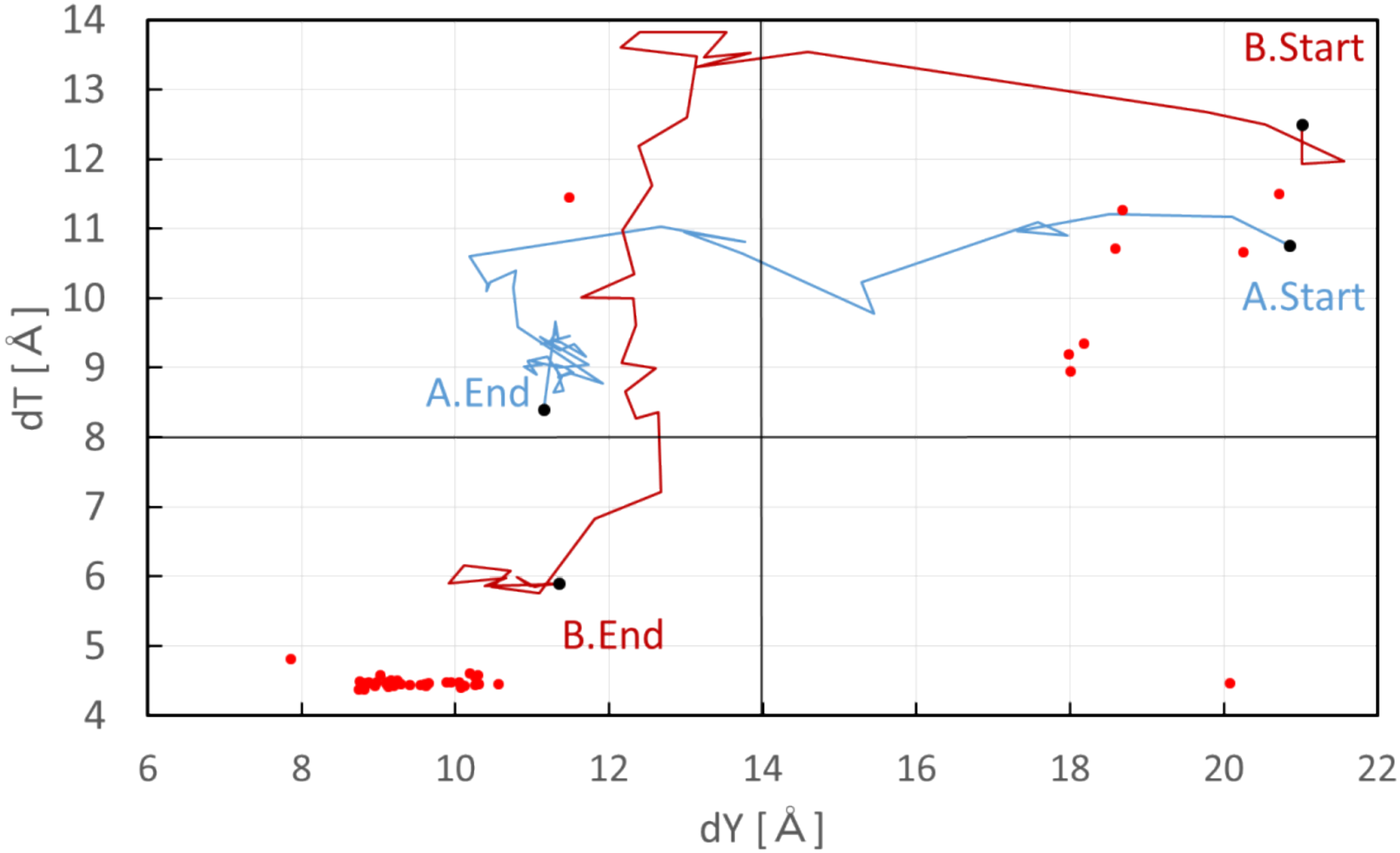
B.Start
A.Start
A.End
B.End
dT [ Å ]
dY [ Å ]
14
13
12
11
10
9
8
7
6
5
4
6
8
10
12
14
16
18
20
22

Figure 2

(a)

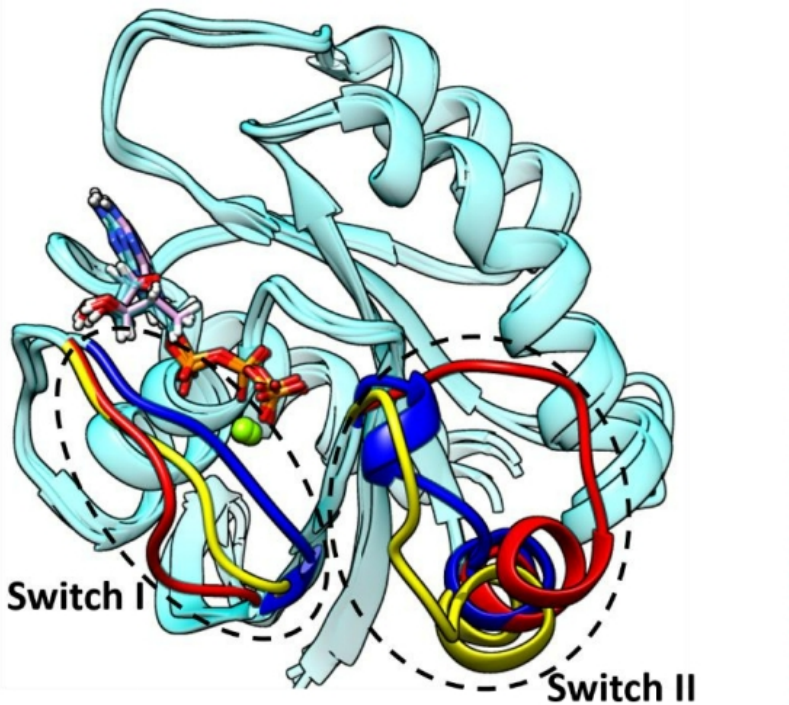


(b)

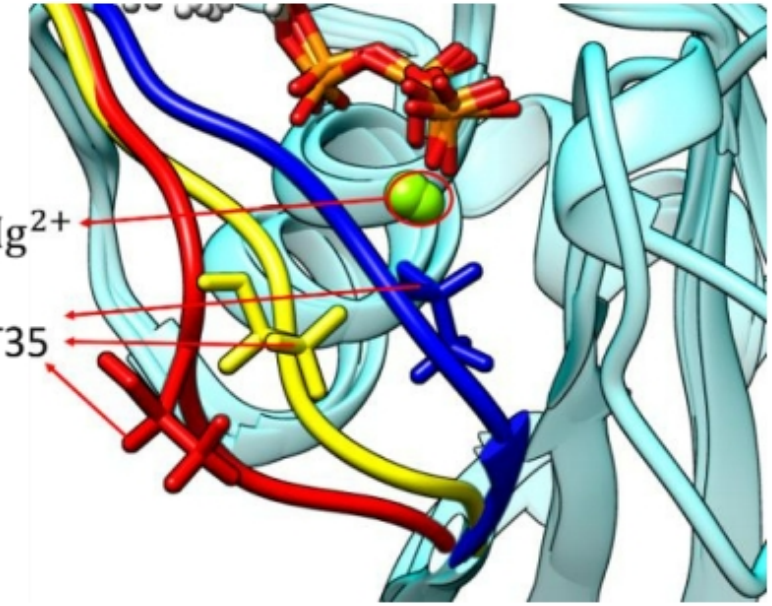


(c)

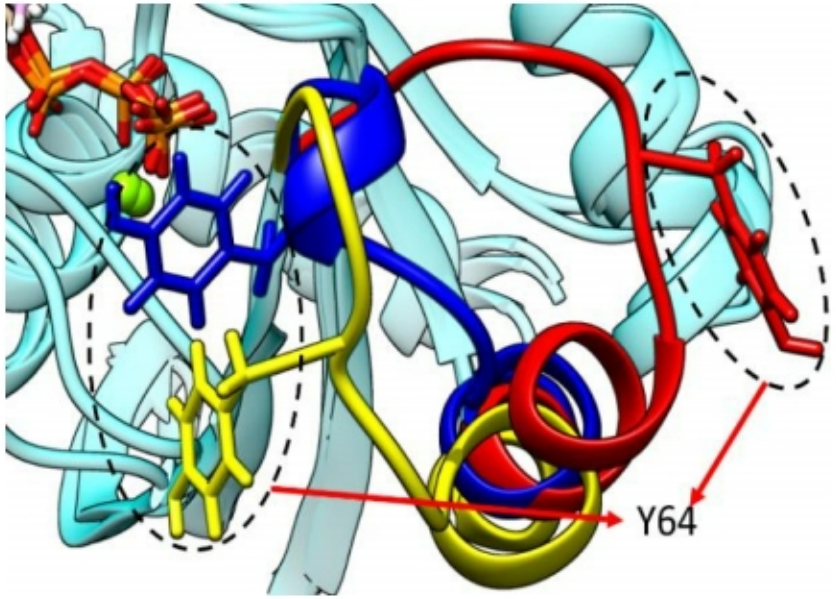


(d)

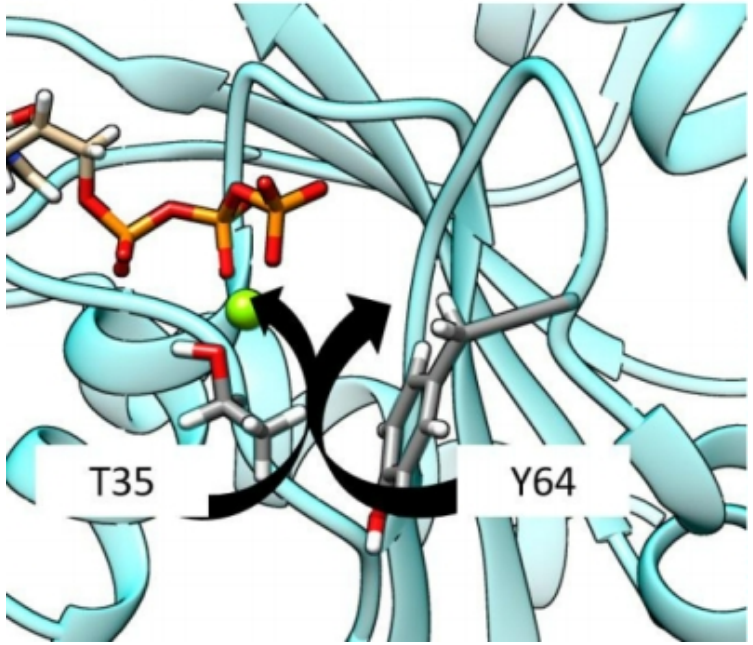


Figure 3

(a)

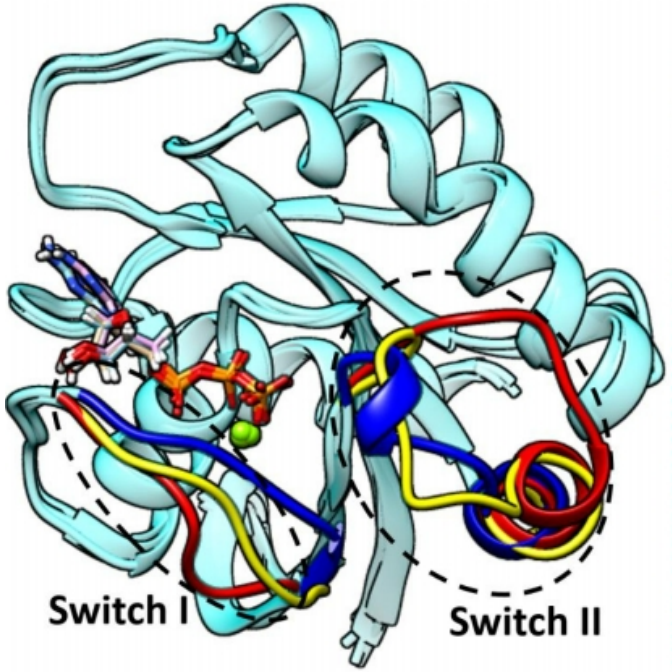


(b)

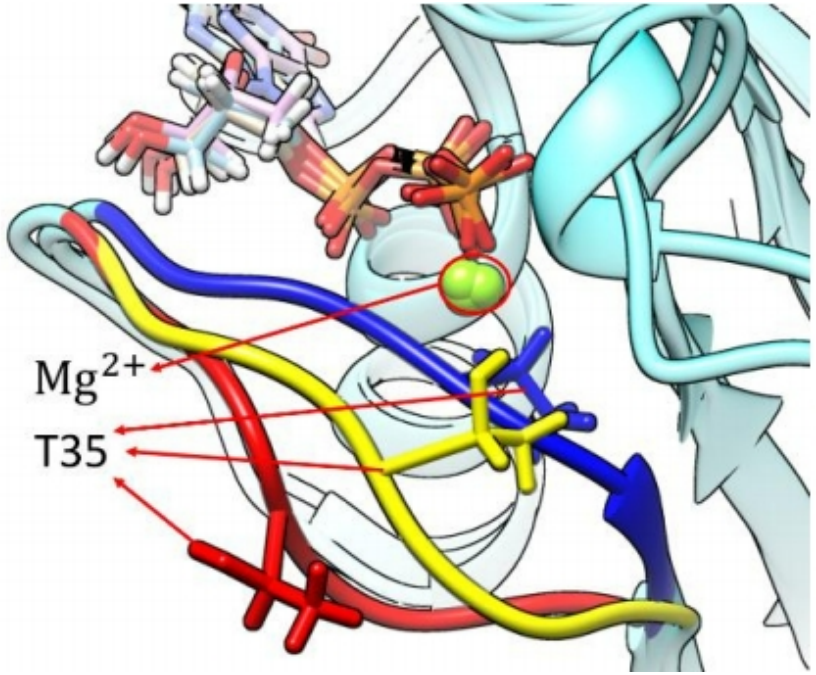


(c)

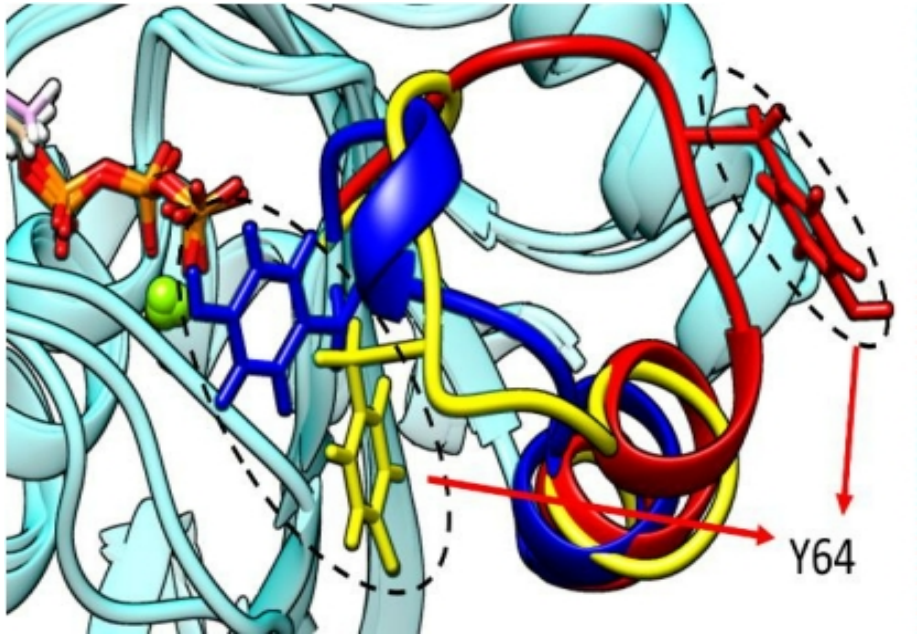


(d)

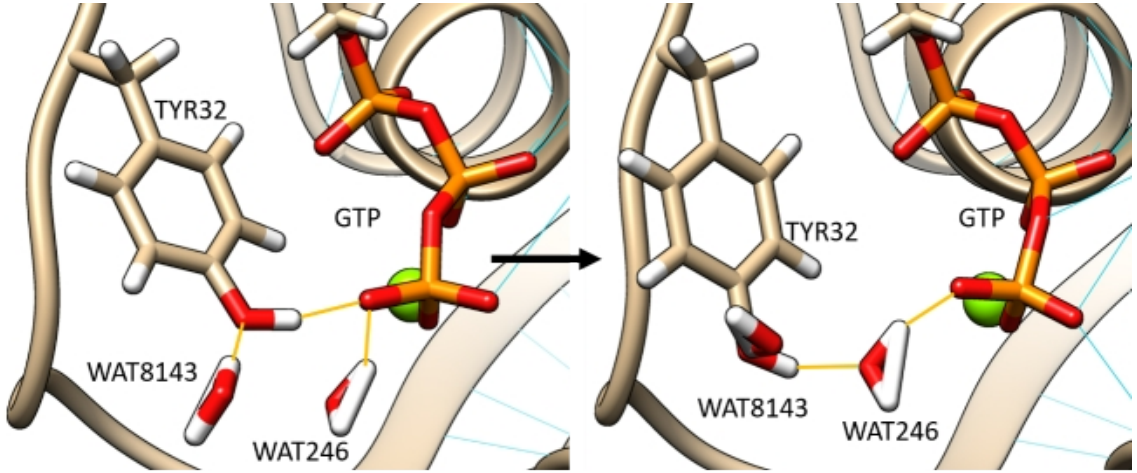


Figure 4

(a)

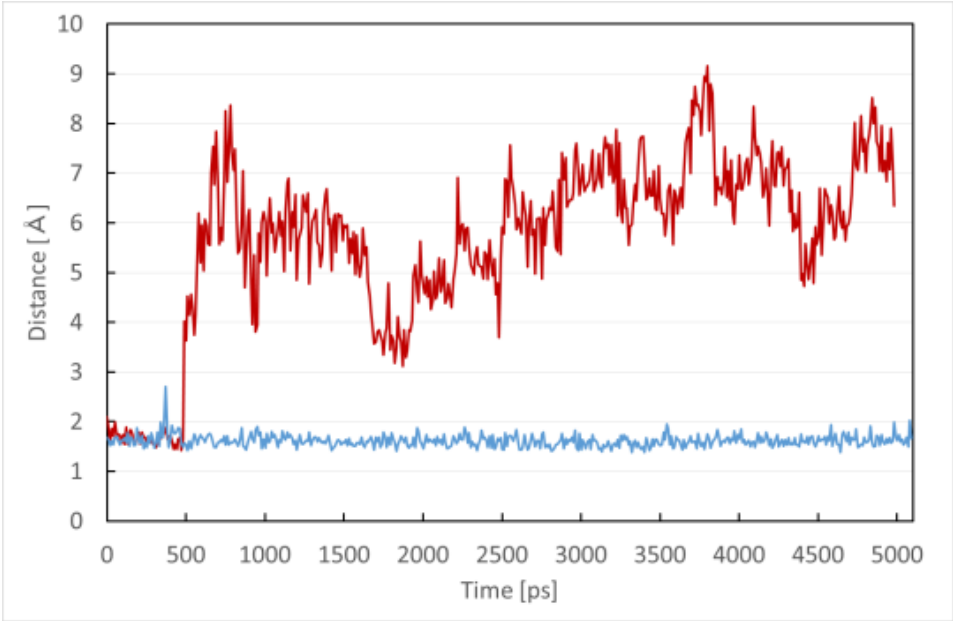
Distance [Å]
Time [ps]
0
1
2
3
4
5
6
7
8
9
10
0
500
1000
1500
2000
2500
3000
3500
4000
4500
5000

(b)

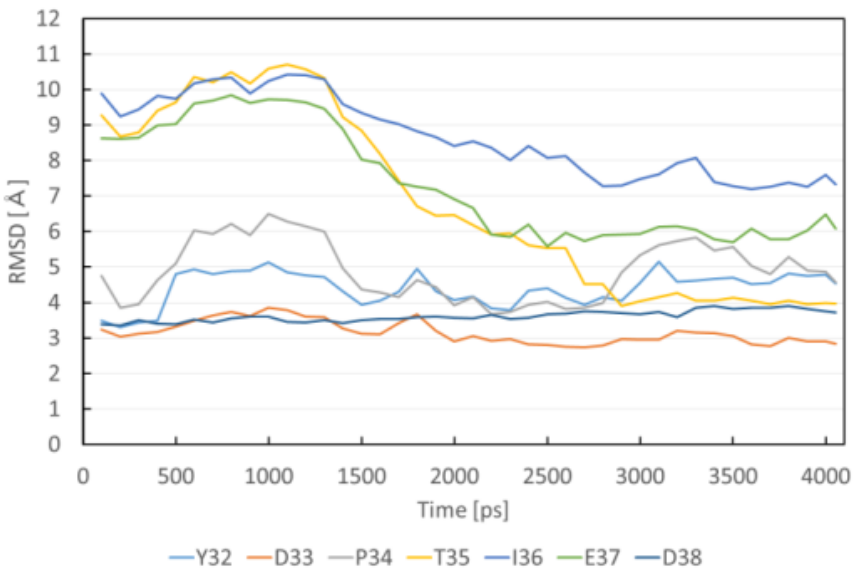
RMSD [Å]
Time [ps]
0
1
2
3
4
5
6
7
8
9
10
11
12
0
500
1000
1500
2000
2500
3000
3500
4000
Y32
D33
P34
T35
I36
E37
D38

(c)

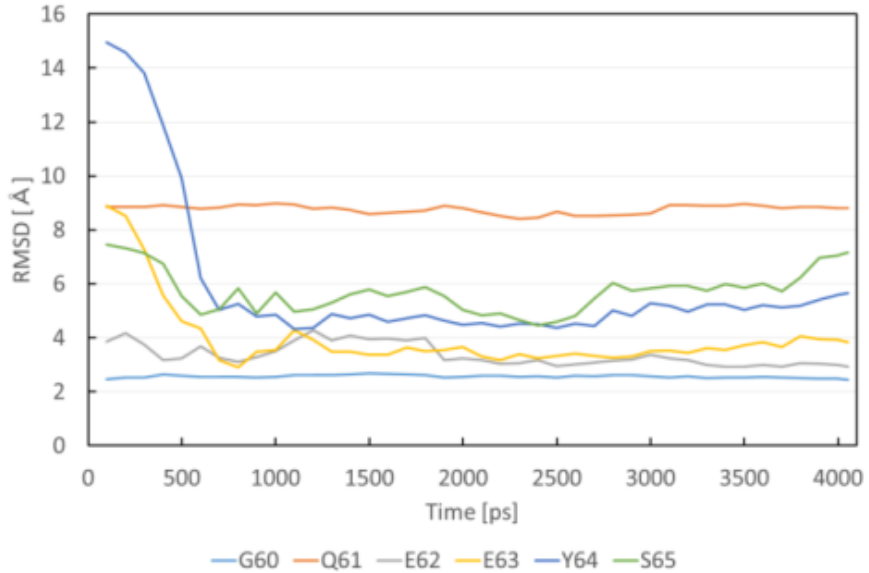
RMSD [Å]
Time [ps]
0
2
4
6
8
10
12
14
16
0
500
1000
1500
2000
2500
3000
3500
4000
G60
Q61
E62
E63
Y64
S65

Figure 5

(a)

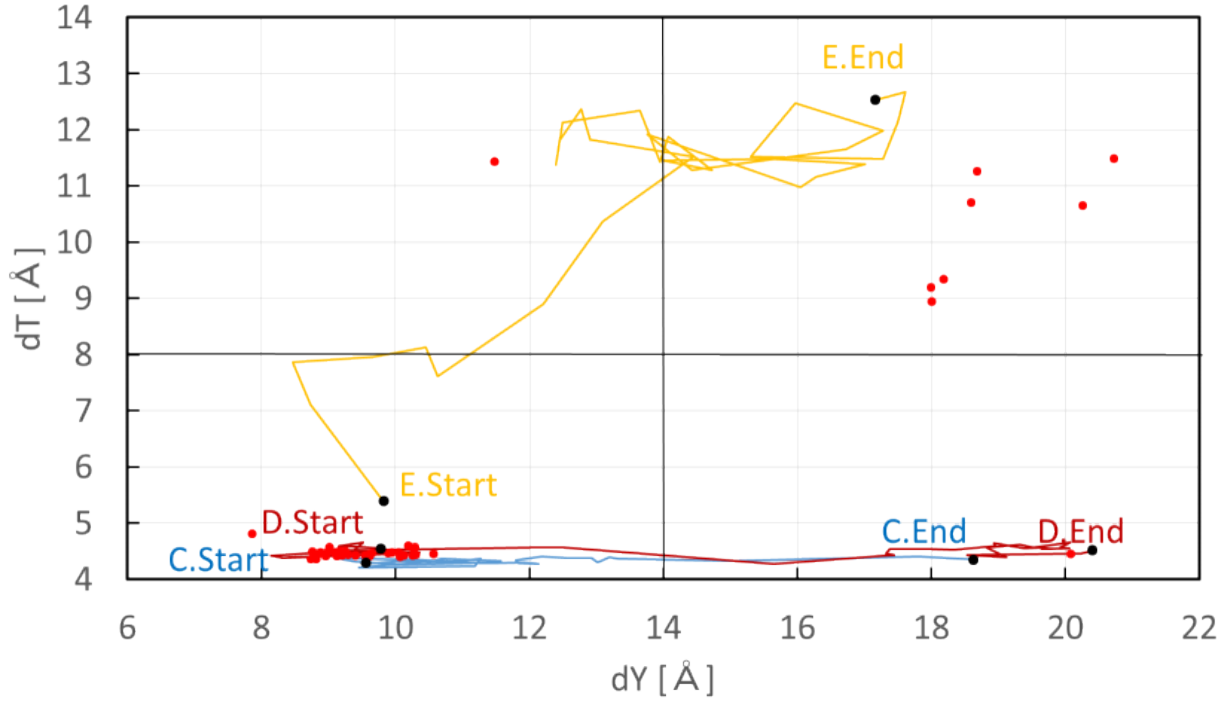
E.End
E.Start
D.Start
C.Start
C.End
D.End
dT [Å]
dY [Å]

(b)

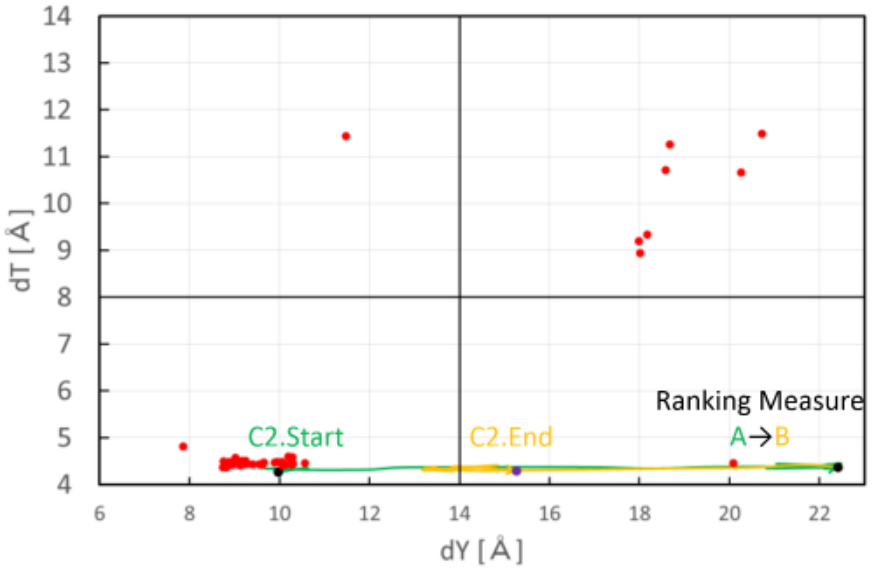
C2.Start
C2.End
Ranking Measure
A→B
dT [Å]
dY [Å]

(c)

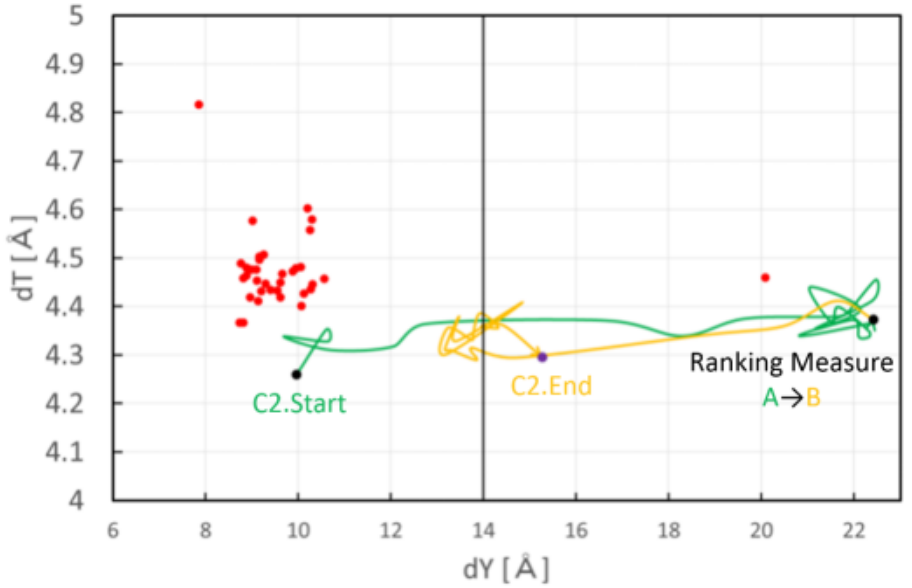
C2.Start
C2.End
Ranking Measure
A→B
dT [Å]
dY [Å]

Figure 6

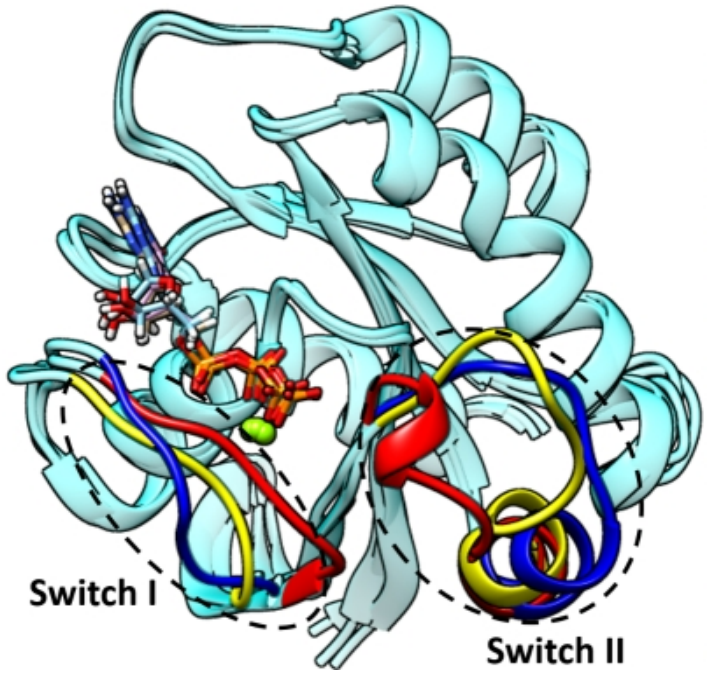


(a)

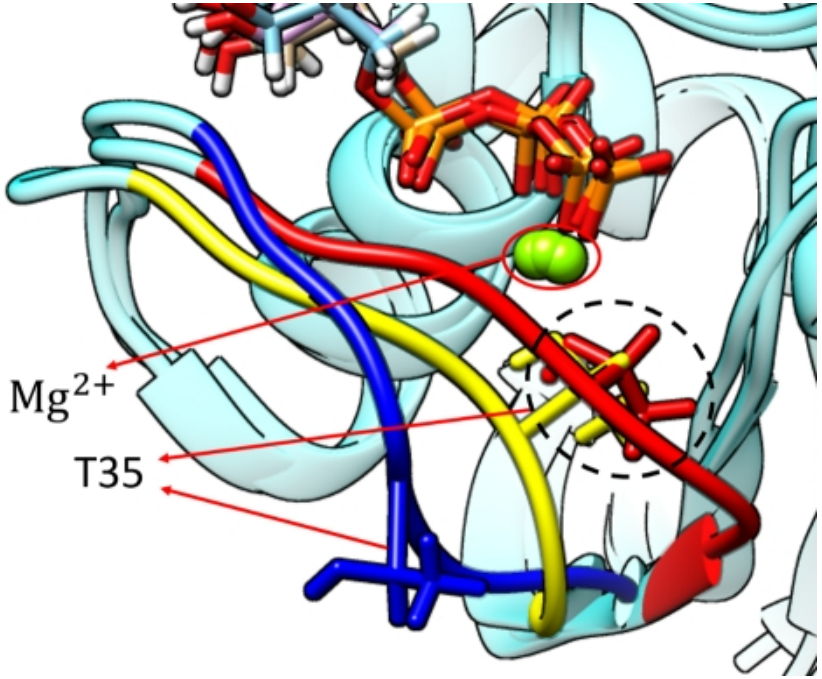


(b)

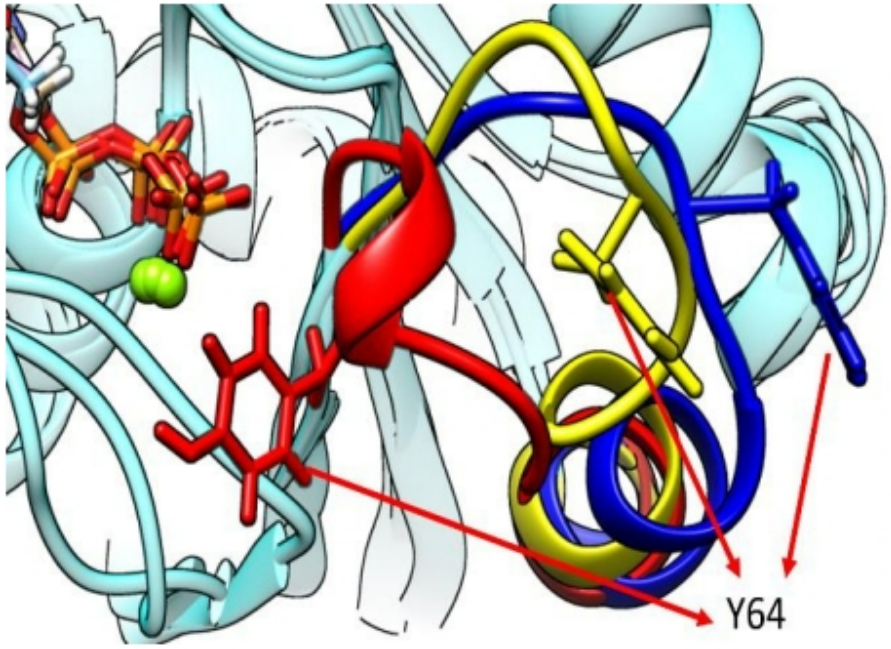


(c)

Figure 7

(a)

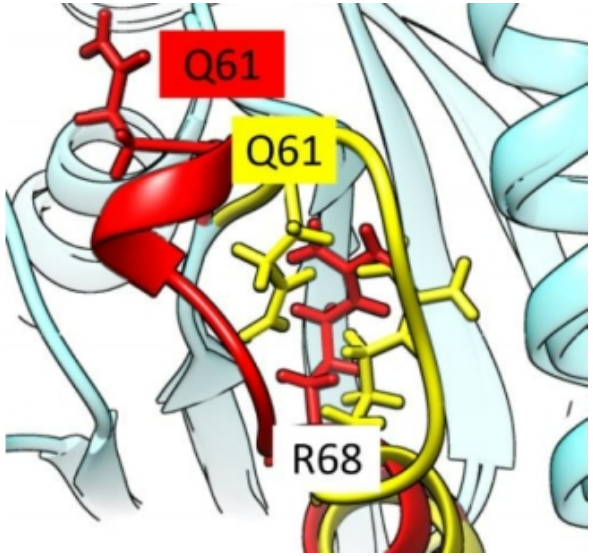


(b)

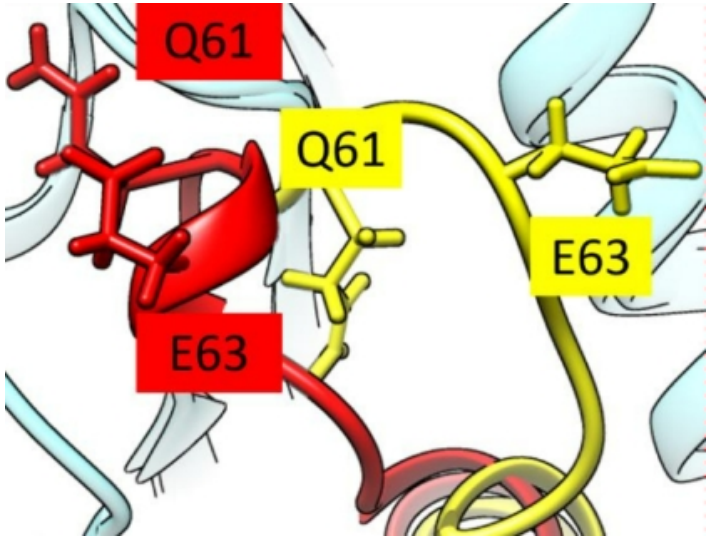


(c)

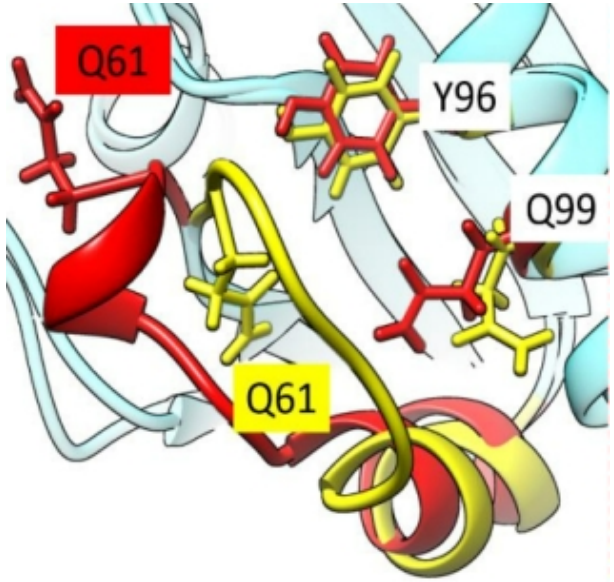


(d)

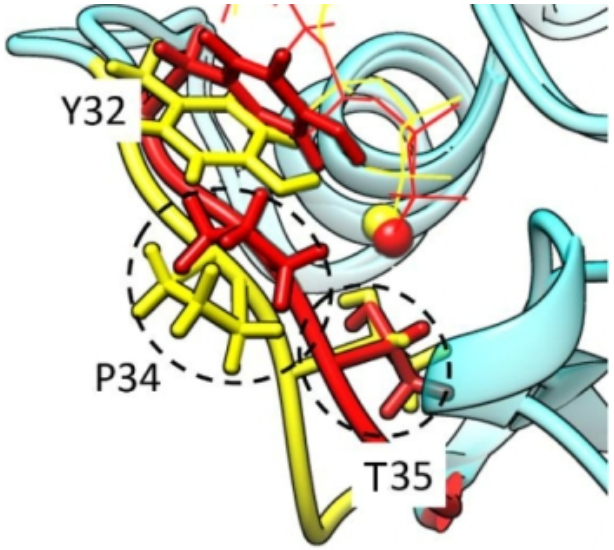


Figure 8

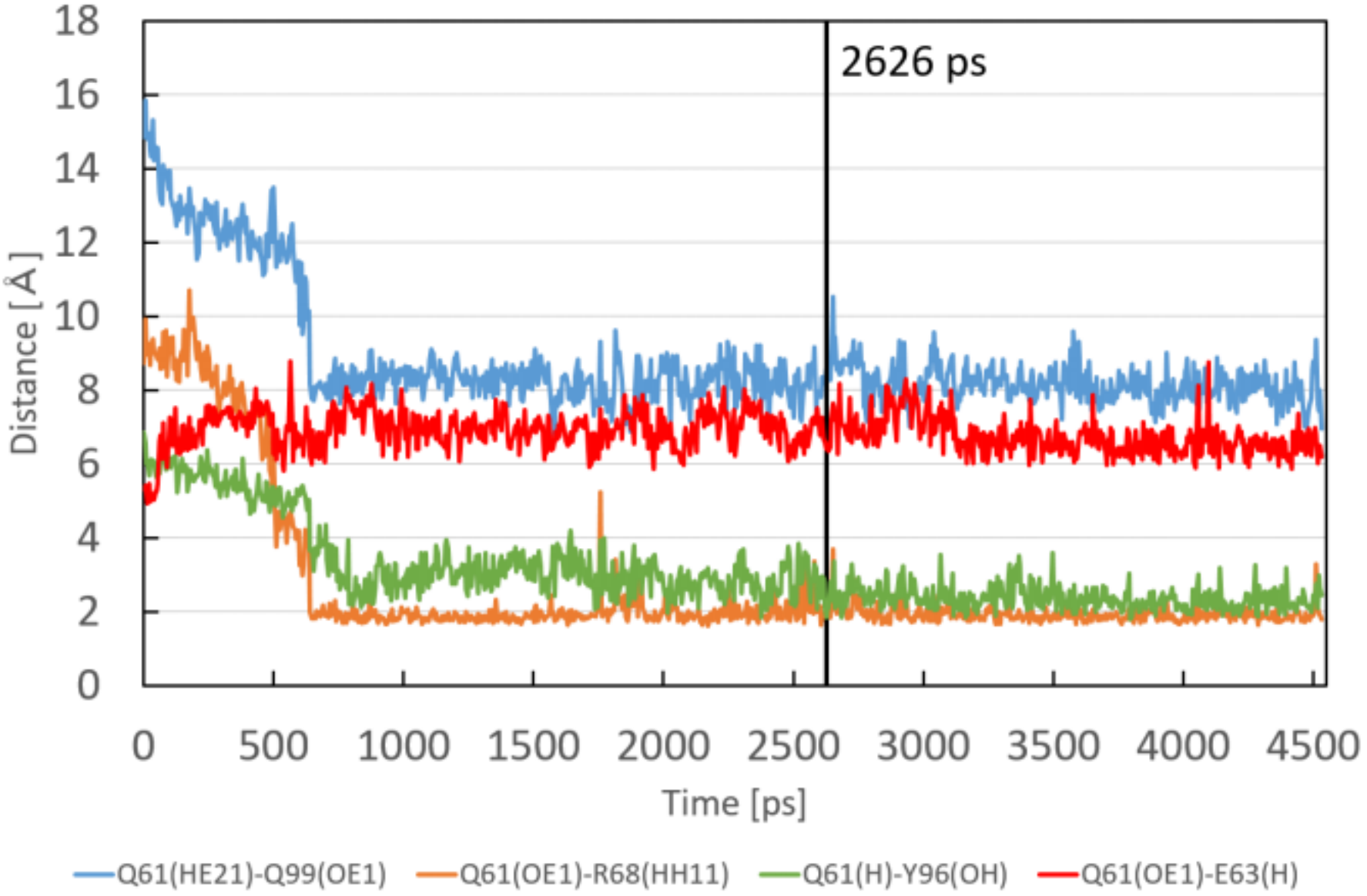
2626 ps
Distance [Å]
Time [ps]
0
2
4
6
8
10
12
14
16
18
0
500
1000
1500
2000
2500
3000
3500
4000
4500
Q61(HE21)-Q99(OE1)
Q61(OE1)-R68(HH11)
Q61(H)-Y96(OH)
Q61(OE1)-E63(H)

Figure 9

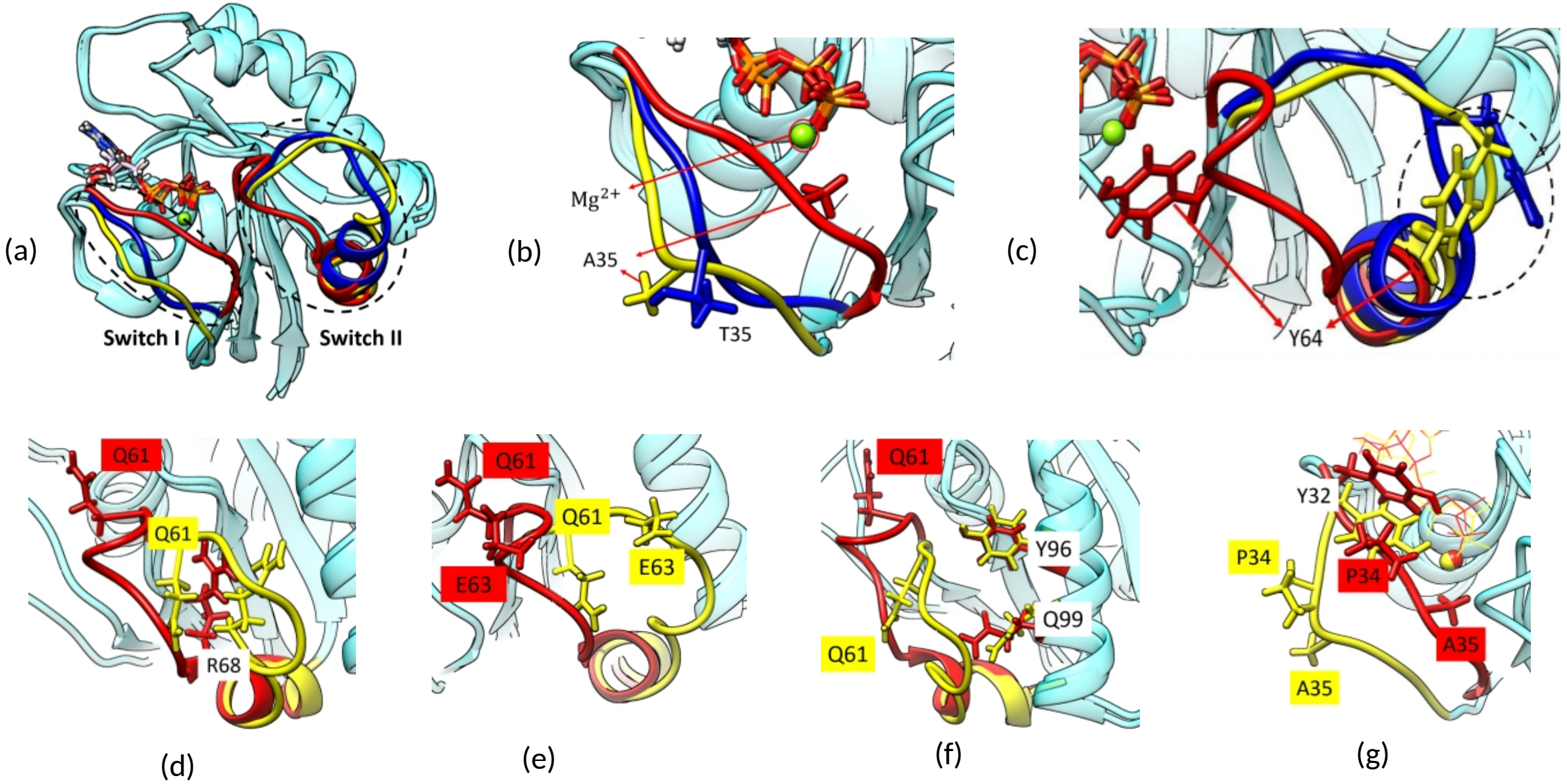
(a)
Switch I
Switch II
(b)
Mg2+
A35
T35
(c)
Y64
Q61
Q61
R68
(d)
Q61
Q61
E63
E63
(e)
Q61
Y96
Q99
Q61
(f)
Y32
P34
P34
A35
A35
(g)

Figure 10

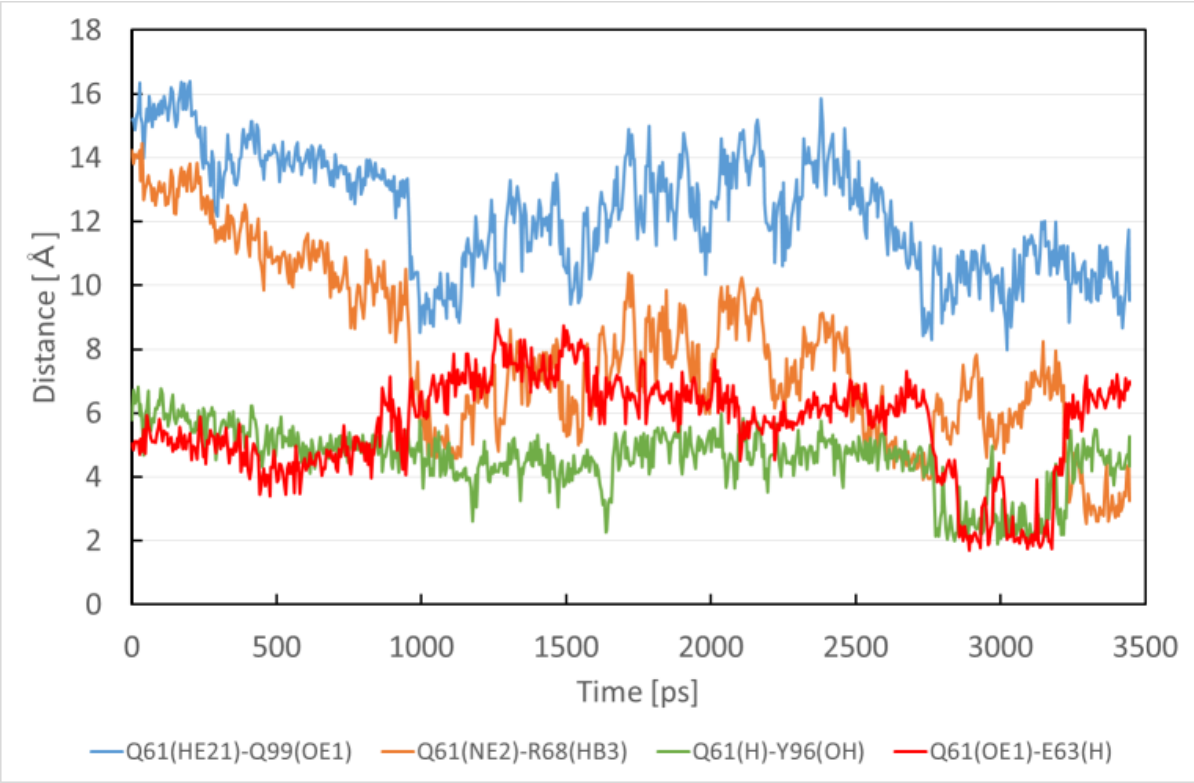
Distance [Å]
Time [ps]
Q61(HE21)-Q99(OE1)
Q61(NE2)-R68(HB3)
Q61(H)-Y96(OH)
Q61(OE1)-E63(H)

(a)

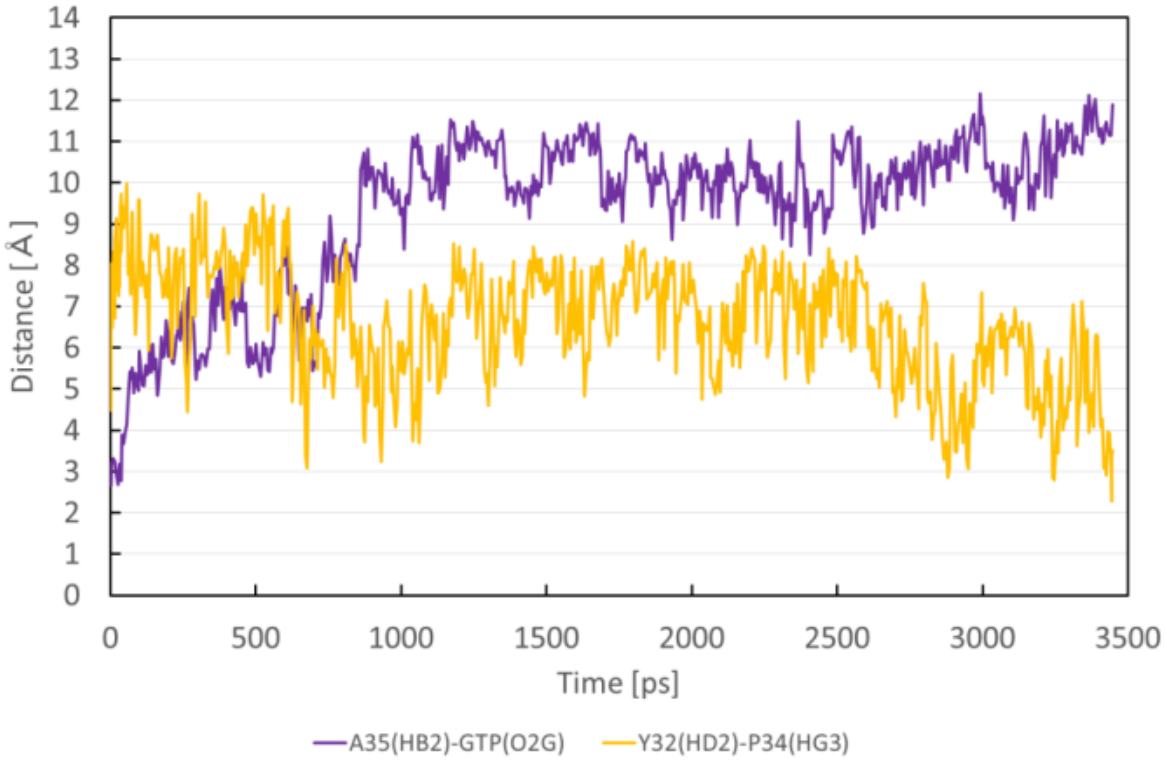
Distance [Å]
Time [ps]
A35(HB2)-GTP(O2G)
Y32(HD2)-P34(HG3)

(b)

Figure 11

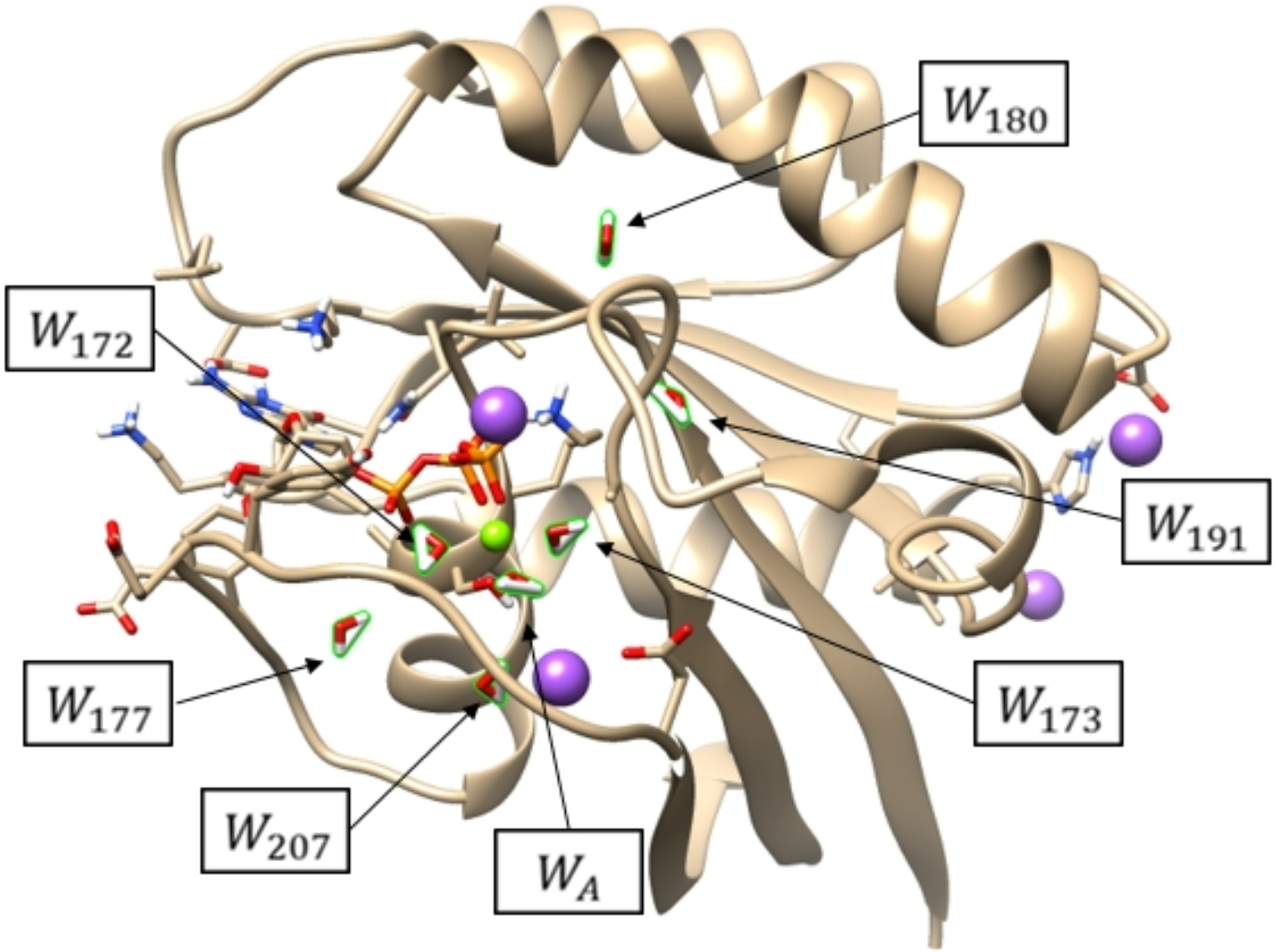


Figure 12

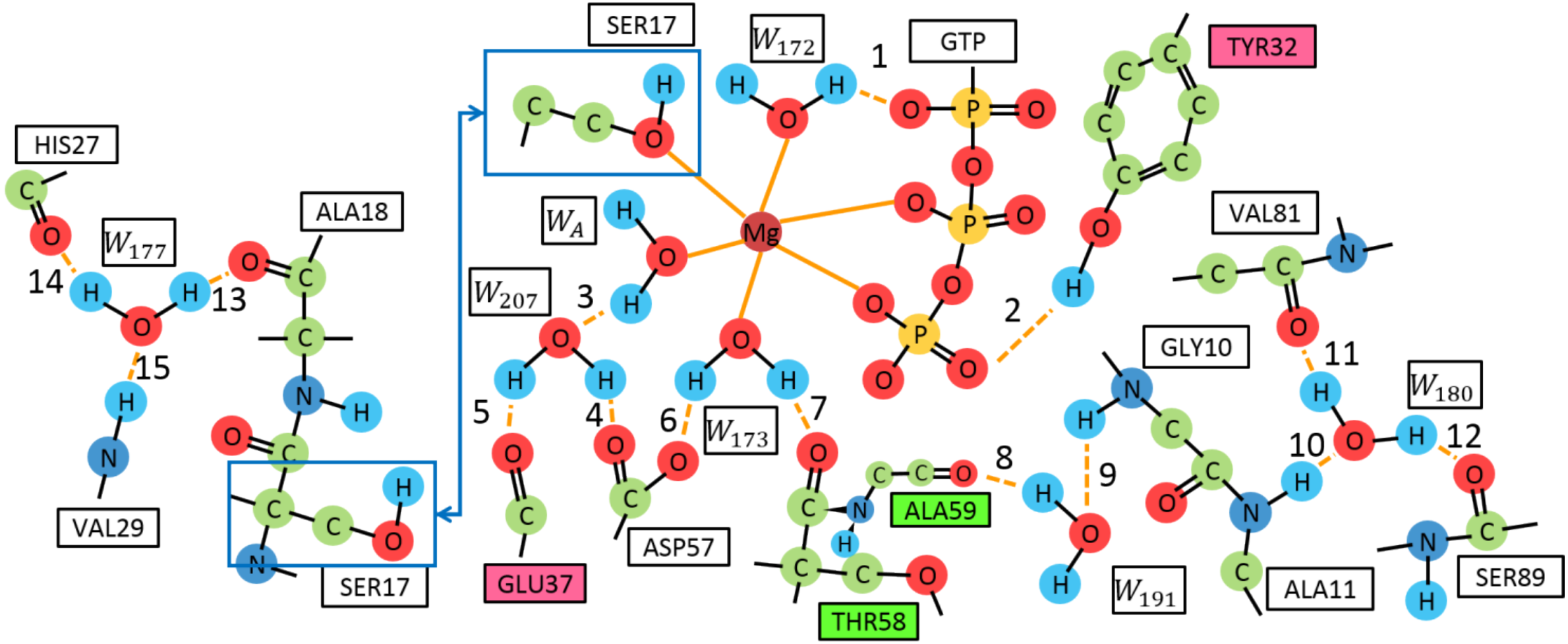
SER17
$W_{172}$
GTP
TYR32
HIS27
ALA18
$W_{177}$
$W_A$
Mg
VAL81
$W_{207}$
GLY10
$W_{180}$
$W_{173}$
ASP57
ALA59
$W_{191}$
ALA11
SER89
VAL29
SER17
GLU37
THR58
1
2
3
4
5
6
7
8
9
10
11
12
13
14
15

Figure 13

(a)

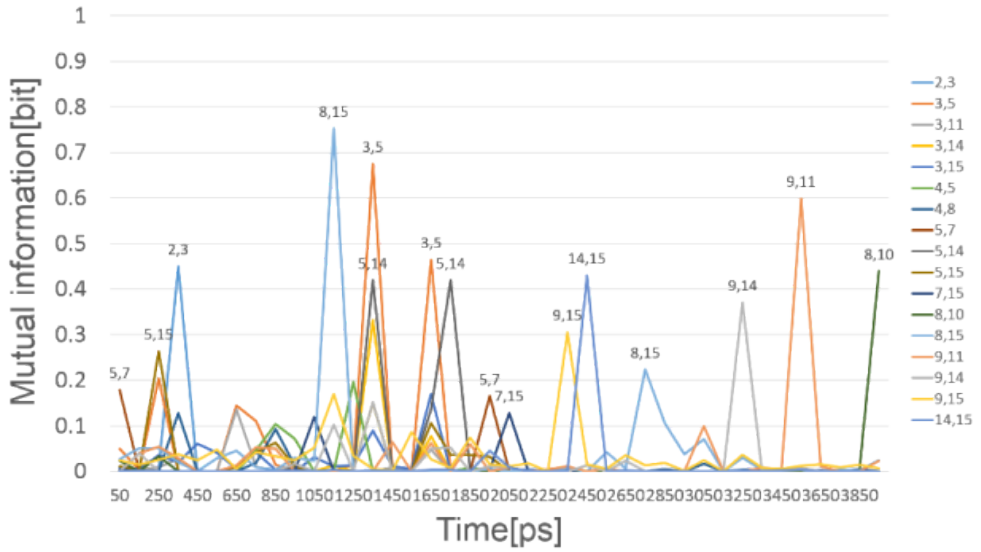


(b)

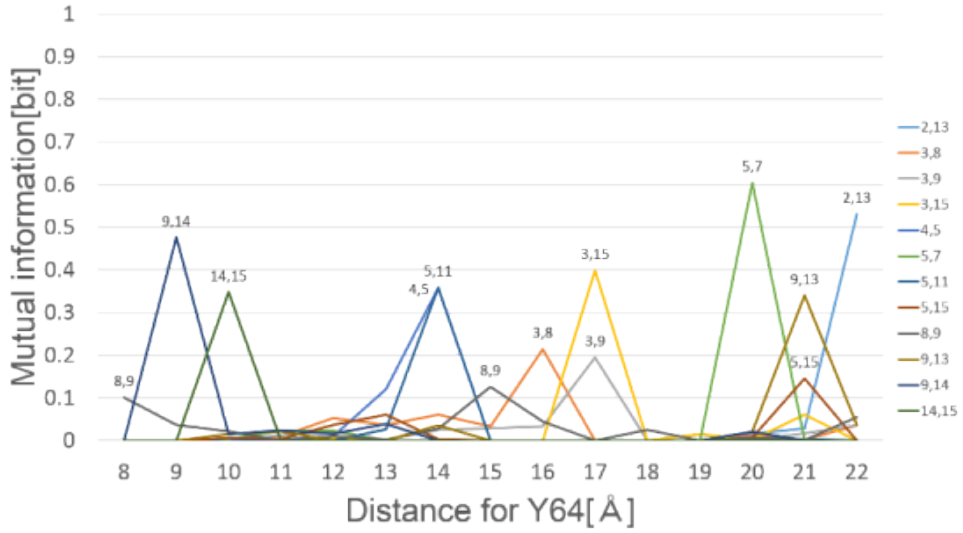


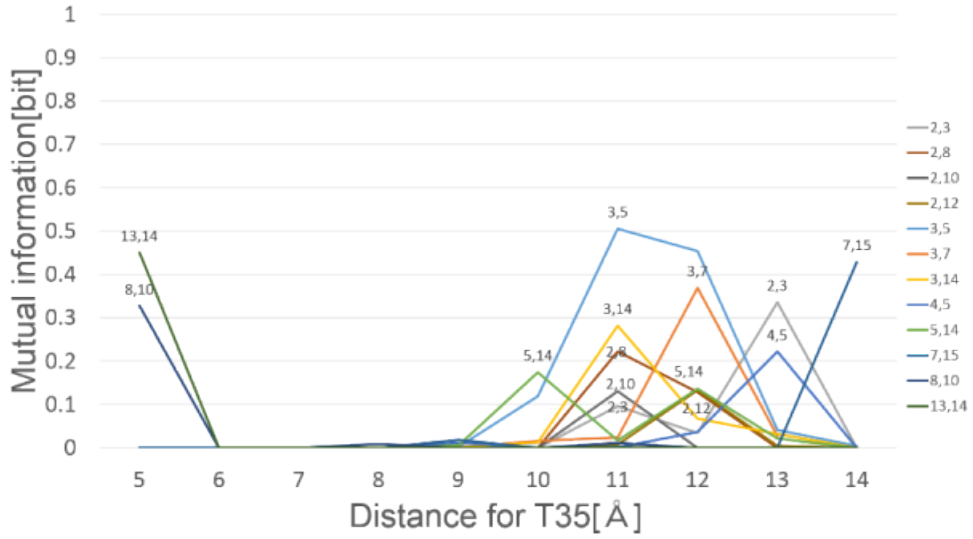


(c)

Figure 14

(a)

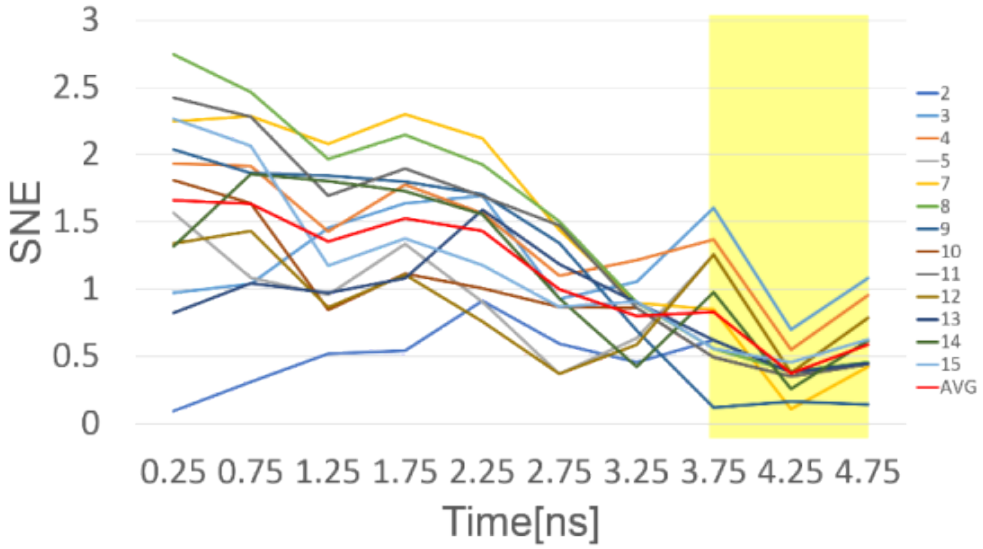


(b)

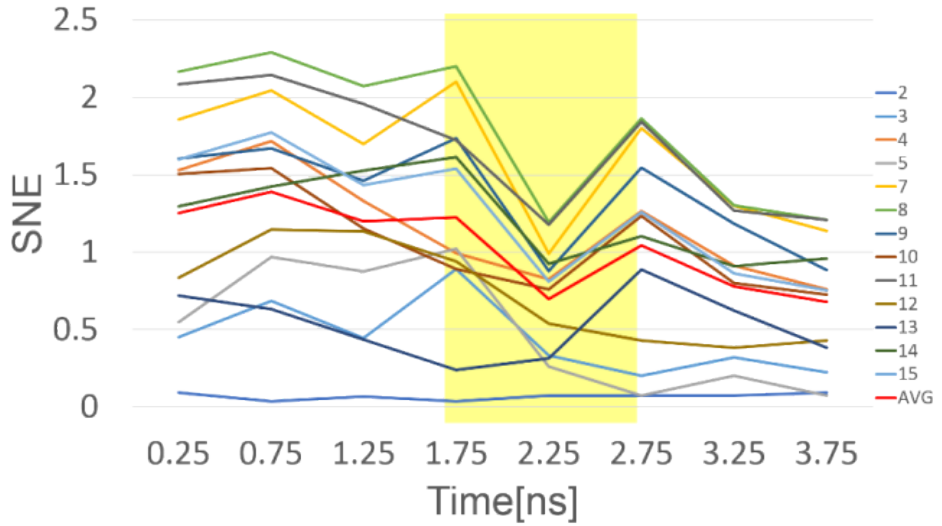


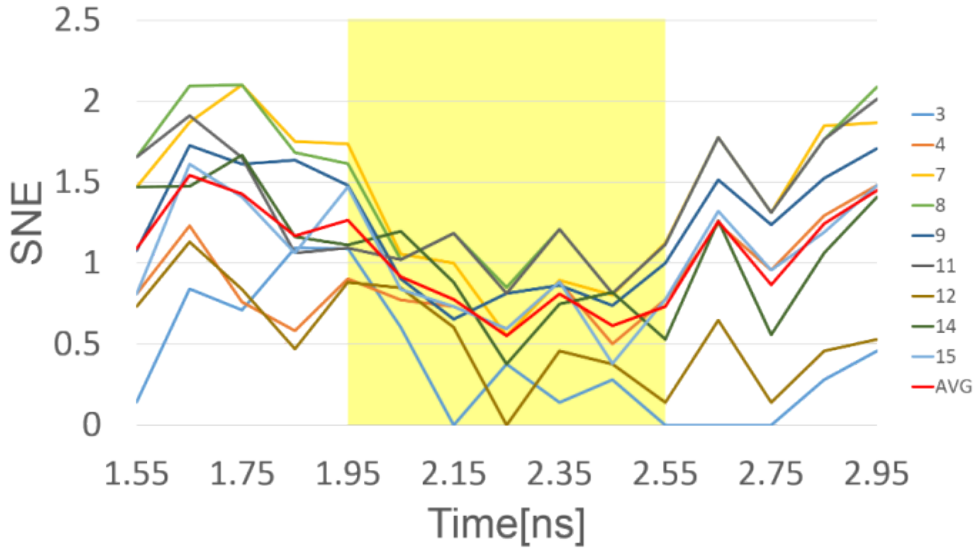


(c)

Figure 15

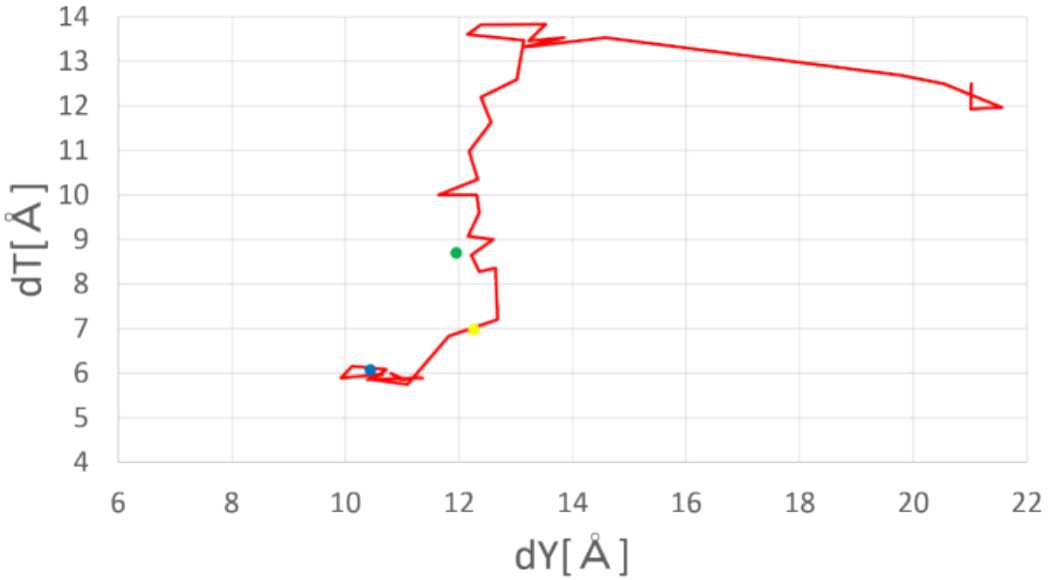


(a)

(b)

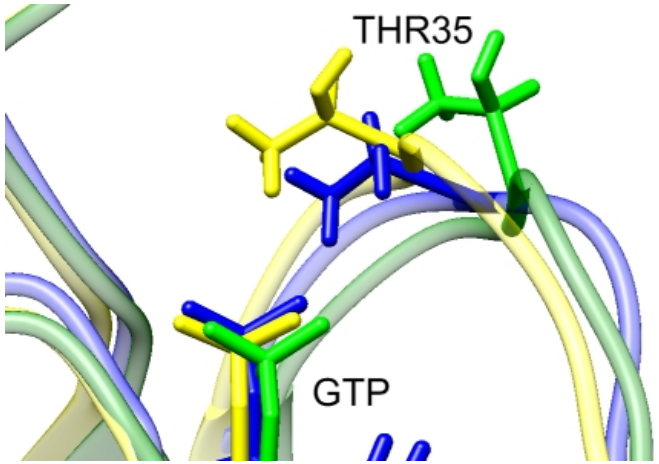


(c)

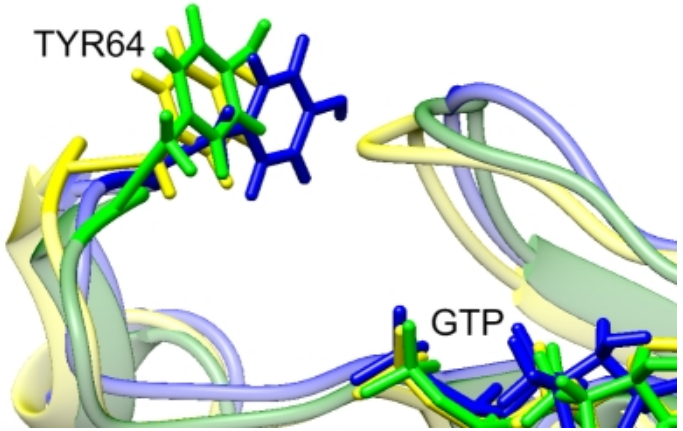


Figure 16

# Supplementary data for Structural transition of solvated H-Ras/GTP revealed by molecular dynamics simulation and local network entropy

Shota Matsunaga, Yuta Hano, Yuta Saito

*Department of Computational Science, Graduate School of System Informatics, Kobe University, 1-1 Rokkodai-cho, Nada-ku, Kobe 657-8501, Japan*

Kazuhiro J. Fujimoto

*Faculty of Pharmaceutical Sciences, Hokuriku University, Ho-3 Kanagawa-machi, Kanazawa 920-1181, Japan*

Takashi Kumasaka

*Protein Crystal Analysis Division, Japan Synchrotron Radiation Research Institute (JASRI), SPring-8, 1-1-1 Kouto, Sayo-cho, Sayo-gun, Hyogo 679-5198, Japan*

Shigeyuki Matsumoto, Tohru Kataoka

*Division of Molecular Biology, Department of Biochemistry and Molecular Biology, Graduate School of Medicine, Kobe University, 7-5-1 Kusunoki-cho, Chuo-ku, Kobe 650-0017, Japan*

Fumi Shima

*Division of Molecular Biology, Department of Biochemistry and Molecular Biology, Graduate School of Medicine, Kobe University, 7-5-1 Kusunoki-cho, Chuo-ku, Kobe 650-0017, Japan; Drug Discovery Science, Division of Advanced Medical Science, Department of Science, Technology and Innovation, Graduate School of Science, Technology and Innovation, Kobe University, 7-5-1 Kusunoki-cho, Chuo-ku, Kobe 650-0017, Japan*

Shigenori Tanaka

*Department of Computational Science, Graduate School of System Informatics, Kobe University, 1-1 Rokkodai-cho, Nada-ku, Kobe 657-8501, Japan*

*Email address:* tanaka2@kobe-u.ac.jp; Fax:+81-78-803-6621 (Shigenori Tanaka)

**Abstract**

Detailed structural data on the crystals of i61a are given in this Supplementary data.

## 1. Structural data of i61a

Crystals of i61a were prepared with the dehydration of crystals using HAG method [1], which is the same protocol as in State 1 crystals (5B30) except no cryopreservation [2]. Although the overall structure is similar to State 1 (5B30), the electron density map corresponding to its Switch II region (residues 61-71) clearly shows partially closed conformation that is rather similar to State 2 (5B2Z). Nevertheless, its electron density is lower in the level, therefore the validity of this current atomic model (i61a) might be lower and the region still contains some Ramachandran outliers. Detailed crystallographic data for H-Ras i61a are given in Table S1.

## References

[1] S. Baba, T. Hoshino, L. Ito, T. Kumasaka, Humidity control and hydrophilic glue coating applied to mounted protein crystals improves X-ray diffraction experiments, Acta Cryst. D 69 (2013) 1839-1849.

[2] S. Matsumoto, N. Miyano, S. Baba, J. Liao, T. Kawamura, C. Tsuda, A. Takeda, M. Yamamoto, T. Kumasaka, T. Kataoka, F. Shima, Molecular mechanism for conformational dynamics of Ras · GTP elucidated from in-situ structural transition in crystal, Sci. Rep. 6 (2016) 1-12.

**Table**

Table S1. Crystallographic analysis of H-Ras i61a.

| | H-Ras (1-166) i61a |
|---|---|
| X-ray source | SPring-8 BL38B1 |
| Space group | *H32* |
| Unit cell (Å) *a, c* | 93.03, 123.20 |
| Wavelength (Å) | 1.02 |
| Resolution (Å) | 50.0-2.79 (2.89-2.79) |
| $R_{merge}$ | 0.134 (0.697) |
| Completeness | 1.0 (1.0) |
| Mean $I/\sigma_I$ | 21.7 (5.6) |
| Number of observed reflections | 33,943 |
| Unique reflections | 5,287 (511) |
| Number of atoms, Protein/Ligand /Wat | 1,323/39/79 |
| $R_{work}/R_{free}$ | 0.172/0.220 |
| Rmsd for bonds | 0.021 |
| Rmsd for angles | 2.00 |
| Ramachandran favoured/outliers (%) | 92.1/4.3 |
| Average $B$ factor, Protein/Ligand/Wat | 29.5/24.7/42.6 |